

# Particle-Guided Diffusion Models for Partial Differential Equations

Andrew Millard<sup>1</sup> Fredrik Lindsten<sup>1</sup> Zheng Zhao<sup>1</sup>

## Abstract

We introduce a guided stochastic sampling method that augments sampling from diffusion models with physics-based guidance derived from partial differential equation (PDE) residuals and observational constraints, ensuring generated samples remain physically admissible. We embed this sampling procedure within a new Sequential Monte Carlo (SMC) framework, yielding a scalable generative PDE solver. Across multiple benchmark PDE systems as well as multiphysics and interacting PDE systems, our method produces solution fields with lower numerical error than existing state-of-the-art generative methods.

## 1. Introduction and Related Work

Partial differential equations (PDEs, Evans, 2022; Strauss, 2007) form the foundation of scientific and engineering models (Ames, 2016), governing phenomena such as fluid flow (Naz et al., 2008), heat transport (Crank & Nicolson, 1947), elasticity (Smith, 1990), electromagnetics (Maxwell, 1865), and the ability to accurately solve PDEs is thus a key enabler for scientific and engineering progress across a broad range of applications (Zachmanoglou & Thoe, 1986). Classical numerical solvers, such as including finite difference (LeVeque, 2007), finite element (Johnson, 2009), and spectral methods (Trefethen, 2000), provide reliable and well-understood approximations, but their computational cost grows rapidly with problem size, nonlinear dynamics, and parameter variability. As a result, simulations in high resolution or across large parameter spaces remain prohibitively expensive for real-time, uncertainty-aware, or many-query settings.

Recent efforts have explored machine learning techniques to accelerate PDE solution. Physics-informed neural networks (PINNs, Cai et al., 2021a;b; Raissi et al., 2019) embed the governing equations into a neural-network loss function and can learn solution fields in addition with observation

<sup>1</sup>Department of Computer and Information Science, Linköping University, Linköping, Sweden. Correspondence to: Andrew Millard <andmi73@liu.se>.

data. Operator-learning models, such as Fourier Neural Operators (Li et al., 2021; 2023) and DeepONets (Lu et al., 2019; 2021), aim to learn mappings from forcing terms or parameters to full-solution fields and enable fast and flexible inference once trained. Neural surrogates, e.g., (Kochkov et al., 2021; Sanchez-Gonzalez et al., 2020), replace expensive numerical methods with models learned from simulations and reduced-order models (Tripathy & Bilionis, 2018; White et al., 2019; Eason & Cremaschi, 2014) further accelerate computation by approximating fine-resolution solutions using coarse representations refined by learned corrections. However, these ML-based PDE solvers produce deterministic predictions (Huang et al., 2024) and may require large datasets or costly hyperparameter tuning. Ensuring physical consistency and robustness across varying boundary conditions and parameter regimes remains challenging, motivating the exploration of probabilistic and generative approaches for forward PDE modeling.

In parallel, flow-based generative models based on diffusion (Song et al., 2021) and stochastic interpolants (Albergo et al., 2025) have emerged as state-of-the-art tools for sampling from complex, high-dimensional distributions. These models gradually transform noise into structured samples via stochastic differential equations, enabling diverse and uncertainty-aware generation in domains such as images (Rombach et al., 2022; Dhariwal & Nichol, 2021), audio (Kong et al., 2021; Huang et al., 2023; Liu et al., 2023), and molecular design (Guo et al., 2024; Yim et al., 2024). Their probabilistic formulation allows sampling from full posterior distributions rather than returning a single point estimate. These properties make diffusion models a promising candidate for scientific simulation, where multiple physically valid solutions may exist.

### 1.1. Related Work

Within the generative modeling literature, various methods have been applied to solving PDEs which can be broadly separated into two different categories: *data driven* and *physics-informed*.

The data driven approach models the underlying relationship between inputs and outputs by discovering correlations and patterns directly from the data without explicitly prescribing physical laws. In the context of PDEs, many

generative methods have attempted to use the data driven approach. For instance, variational Autoencoders and generative adversarial networks have been used extensively to model PDEs (Gonzalez & Balajewicz, 2018; Creswell et al., 2018; Barati Farimani et al., 2017; Mirza & Osindero, 2014). Flow-based generative models have also found success recently in this area, with applications in fluid field prediction (Yang & Sommer, 2023; Kohl et al., 2024; Liu & Thurey, 2024), weather forecasting (Price et al., 2025), 3-dimensional turbulent flows (Molinaro et al., 2024), modeling buoyancy (Li et al., 2025).

Physics-informed approaches are common in the PINN literature (Cai et al., 2021a;b; Raissi et al., 2019) but have seen less common adoption by the generative modeling community. Lienen et al. (2024) utilize Dirichlet boundary conditions as guidance when sampling, but do not incorporate the full equations as part of a loss function, therefore it is still primarily a data driven approach. Shysheya et al. (2024); Rozet & Louppe (2023) use diffusion models trained on PDE data in combination with inference-time (“zero shot”) guidance for data assimilation, i.e., to condition the generation on sparse measurements. Closest to our work is DiffusionPDE (Huang et al., 2024) which similarly uses guidance to incorporate the governing equations into the likelihood during the sampling process.

The guidance methods used in these frameworks are not specific to PDEs, and many methods have been developed for controlled generation, predominantly in computer vision (see, Daras et al., 2024; Chung et al., 2025, for recent surveys). Motivated by the need for diversity and statistical consistency, several recent contributions incorporate Sequential Monte Carlo (SMC, Wu et al., 2023; Cardoso et al., 2024; Kelvinius et al., 2025; Zhao, 2026) and Markov Chain Monte Carlo (Dang et al., 2025; Janati et al., 2025; Corenflos et al., 2025; Kalaivanan et al., 2025) in the guidance procedure. However, we have yet to see an adaptation of such methodology to physics-informed regularization of generative PDE solvers.

## 1.2. Contributions

We propose a new method for guidance of pretrained generative PDE solvers leveraging SMC for improved efficiency. This enables data assimilation as well as physics-informed regularization for solving constrained PDE systems.

However, while existing SMC-based guidance methods in computer vision and other domains (Wu et al., 2023; Cardoso et al., 2024; Stevens et al., 2025; Dou & Song, 2024; Kelvinius et al., 2025; Zhao et al., 2025) are primarily motivated by statistical consistency, we challenge this interpretation. While these methods indeed show improved empirical performance compared to their non-SMC counterparts, we argue that this is *despite the fact that the SMC algorithms are*

*highly degenerate when applied to conditional generative models.* In other words, we argue that existing SMC-based guidance methods for high-dimensional generative models are effective, not because they achieve a high effective sample size, but due to their inherent “multiple try” sampling nature. We elaborate on this interpretation in Section 3.5.

Based on this insight, our contributions are:

- We develop an SMC-based guidance method for data assimilation and physics-informed regularization for solving constrained PDE systems.
- We propose to use a second order stochastic proposal augmented with PDE guidance (referred to as the SOSaG proposal) for better integration of the diffusion models.
- While the basic SMC-formulation is theoretically consistent, we show that it’s incompatible with the efficient SOSaG proposal. We therefore propose a generalization of the SMC framework that trades statistical consistency for improved empirical performance, effectively resulting in a hybrid “vanilla guidance” and SMC approach.
- We demonstrate that this new method outperforms other guided sampling approaches (Huang et al., 2024) on multiple benchmark datasets, as well as two and three species interacting PDE systems.

## 2. Problem Formulation and Background

### 2.1. Partial Differential Equations

We consider the case for both static and time dependent PDEs. In the static case, for a spatial domain  $\Omega$  a PDE can be written as

$$\begin{aligned} f(c, a, u) &= 0, & c \in \Omega, \\ u(c) &= g(c), & c \in \partial\Omega, \end{aligned} \quad (1)$$

where  $c$  is a spatial coordinate,  $u \in \mathcal{U}$  is the solution field of the PDE, and  $a \in \mathcal{A}$  is a coefficient field that describes some properties of the system which influence the PDE. For example, in Darcy flow, one solves for the pressure field  $u(c)$  given the permeability field  $a(c)$  of a specific medium  $-\nabla \cdot (a(c)\nabla u(c)) = s(c)$  and  $s(c)$  is a source term such as a forcing function. For a time-dependent PDE defined over a time horizon  $[0, \mathcal{T}]$ , we write

$$\begin{aligned} f(c, \tau, a, u) &= 0, & c \in \Omega, \quad \tau \in [0, \mathcal{T}], \\ u(c, \tau) &= g(c, \tau), & c \in \partial\Omega, \quad \tau \in [0, \mathcal{T}], \\ u(c, 0) &= a(c), \end{aligned} \quad (2)$$

where  $\tau$  denotes PDE time (to be distinguished from the denoising diffusion time  $t$ ). Here,  $u$  is the solution field

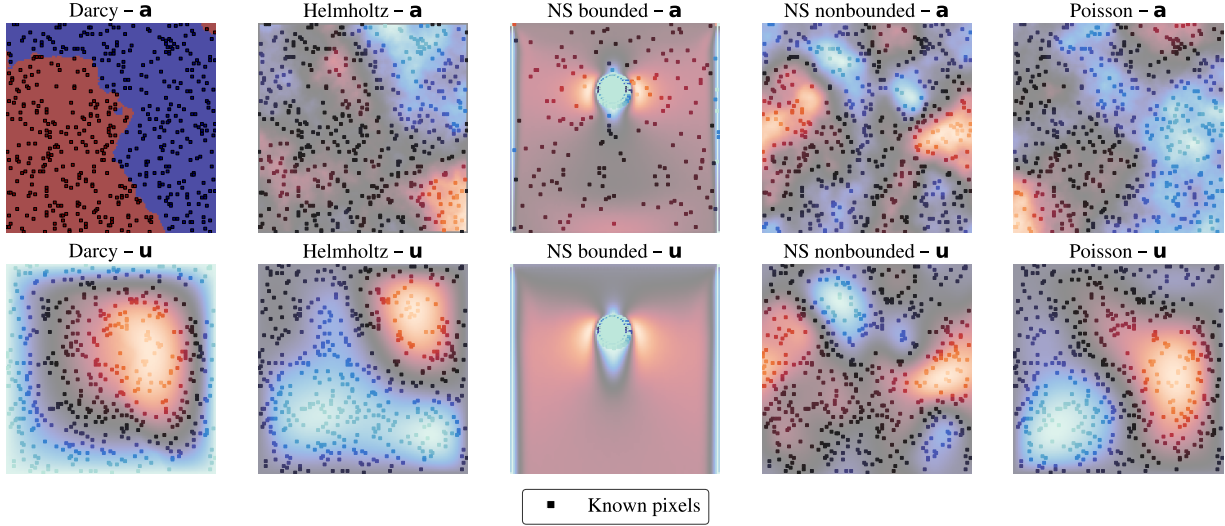


Figure 1. Contour plot of the ground truth parameters overlaid with the observed values (highlighted pixels) for each PDE. The top row shows the coefficient field and the bottom row shows the solution field.

and  $a$  specifies the initial condition and/or PDE coefficients. As an example of such a dynamic system, we consider the incompressible Navier–Stokes (INS) equations, where the solution field is the velocity  $u(c, \tau) = v(c, \tau)$ , together with a pressure field  $p(c, \tau)$ , viscosity  $\nu$ , and external forcing  $q(c, \tau)$ . In this setting, the initial condition is given by  $a(c) = v(c, 0)$ , and our goal is to recover  $a$  and/or the solution at a later time  $u_T = u(\cdot, \mathcal{T})$  from sparse observations.

## 2.2. Sampling for Generative Diffusion Models

Generative diffusion models (Sohl-Dickstein et al., 2015; Song et al., 2021; Ho et al., 2020; Cao et al., 2024; Karras et al., 2022) provide a probabilistic framework for sampling from complex, high-dimensional data distributions  $p_{\text{data}}(x)$ .<sup>1</sup> Over many time steps,  $p_{\text{data}}(x)$  is gradually corrupted by adding Gaussian noise with standard deviation  $\sigma$ , where  $\sigma$  is obtained from a predetermined noise schedule such that  $\sigma_t \in [0, \sigma_{\max}]$  and  $t \in [0, T]$ . Therefore,  $p(x, \sigma_{\max}) = p_{\text{ref}}(x) \approx \mathcal{N}(0, \sigma_{\max}^2 I)$ . In order to generate samples that approximate  $p_{\text{data}}(x)$ , we draw a sample  $x_T \sim \mathcal{N}(0, \sigma_{\max}^2 I)$  and gradually denoise the samples with  $\sigma_t$  so that  $x_t \sim p_t(x_t, \sigma_t)$  and  $x_0 \sim p_{\text{data}}(x)$ .

The probability flow ordinary differential equation (ODE) describes how a sample can be denoised (Song et al., 2021; Karras et al., 2022) in reverse-time according to

$$dx_t = -\dot{\sigma}_t \sigma_t \nabla_{x_t} \log p_t(x_t, \sigma_t) dt, \quad t \in [0, T], \quad (3)$$

where  $\nabla_{x_t} \log p_t(x_t, \sigma_t)$  is the score function, and the forward noising process is considered a Brownian motion as

<sup>1</sup>For consistency, we follow the EDM formulation (Karras et al., 2022), but our methodology can be generalized to other flow-based generative models (Albergo et al., 2025; Lipman et al., 2023).

in Karras et al. (2022). It has previously been proposed (Karras et al., 2022) to learn the denoising function  $D_\theta(x; \sigma)$  such that the score function can be estimated by:

$$\nabla_x \log p_t(x_t, \sigma_t) = \frac{x_t - D_\theta(x_t, \sigma_t)}{\sigma_t^2}. \quad (4)$$

Here,  $D_\theta$  is a neural network trained to predict the denoised version of a noisy sample at a given noise level. Consequently, the score is proportional to the difference between the noisy sample and its denoised estimate, yielding an implicit estimate of the added noise.

An alternative to ODE sampling is to simulate the reverse-time stochastic differential equation (SDE), described by

$$dx_t = -2\dot{\sigma}_t \sigma_t \nabla_{x_t} \log p_t(x_t, \sigma_t) dt + \sqrt{2\dot{\sigma}_t \sigma_t} dW_t, \quad (5)$$

where  $W_t$  is a Brownian motion. The derivation of the ODE and SDE equivalence follows from matching the path distribution. Again, a denoising neural network  $D_\theta$  is trained which in turn is used to approximate the score  $\nabla_x \log p_t(x, \sigma_t)$ , enabling approximate inversion of the original noising process through a reverse-time SDE.

## 2.3. Stochastic Guided Sampling for Solving PDEs

In this work we propose to solve PDE equations by using a diffusion model, pretrained on the joint distribution of coefficients  $a$  and solutions  $u$ , similar to Huang et al. (2024). This model acts as a prior distribution and we then use PDE residuals as guidance during inference. Thus, the samples generated by the diffusion model are the tuples  $x = (a, u)$  where

$$x \in \mathcal{X}, \quad \mathcal{X} = \mathcal{A} \times \mathcal{U}, \quad (6)$$

i.e., concatenating the PDE coefficients and solution, and we denote the prior distribution over these tuples by  $p_{\text{data}}$ .

However, naively solving a PDE using this approach is fundamentally no different compared to just generating an image (see, e.g., [Yang & Sommer, 2023](#)), ignoring two crucial information: the governing PDE equation, and often times, sparse observations  $a_{\text{obs}}, u_{\text{obs}}$  of the coefficients and solution. We thus propose to incorporate these information as a condition  $y$  and aim to sample from a conditional/posterior diffusion model. The sampling can be achieved by simulating the conditional diffusion model

$$dx_t = \underbrace{-2\dot{\sigma}_t \sigma_t \nabla_{x_t} \log p_t^\theta(x_t, \sigma_t) dt}_{\text{Score term}} - \underbrace{2\dot{\sigma}_t \sigma_t \nabla_{x_t} \log p_t^\theta(y | x_t, \sigma_t) dt}_{\text{Guidance term}} + \sqrt{2\dot{\sigma}_t \sigma_t} dW_t. \quad (7)$$

In addition to the score term, we note that (7) now has a gradient term based on the conditional information which we call the *guidance* term. This extra term will tilt the unconditional diffusion model at time  $t = 0$ , to the posterior distribution

$$p_\theta(x | y) \propto p(y | x) p_\theta(x), \quad (8)$$

where  $p_\theta(x) \approx p_{\text{data}}$  is given by a pre-trained diffusion model prior. However, exactly targeting this posterior would require computing the intermediate likelihood  $p_t^\theta(y | x_t, \sigma_t) = \int p(y | x_0) p_\theta(x_0 | x_t) dx_t$  which is in general intractable. Different guidance methods ([Dou & Song, 2024](#); [Zhao et al., 2025](#); [Daras et al., 2024](#); [Chung et al., 2025](#)) approximate this intermediate likelihood in different ways. In the next section we introduce Sequential Monte carlo (SMC) which leverages interacting particles as a way to correct the approximation and to form the posterior distribution.

## 2.4. Sequential Monte Carlo

SMC methods (e.g., [Chopin et al., 2020](#); [Naesseth et al., 2019](#)) provide a principled particle-based framework for sampling from a sequence of distributions, and naturally align with the sequential denoising procedure of generative diffusion models. Previous works have used the SMC framework as a conditional sampling algorithm for diffusion models ([Wu et al., 2023](#); [Cardoso et al., 2024](#); [Stevens et al., 2025](#); [Dou & Song, 2024](#); [Kelvinius et al., 2025](#); [Zhao et al., 2025](#)). In the previous sections  $t$  was used when discussing continuous time processes. In reality, when simulating these processes we approximate them in discrete time  $k$  and therefore we shall be using  $k$  in the following sections.

SMC evolves a population of  $N$  particles  $\{x_k^{(i)}\}_{i=1}^N$  across  $k = 0, 2, \dots, K$  time steps. The key components of SMC are the proposal distributions/Markov kernels  $M_K(x_K)$ ,

$\{M_{k-1}(x_{k-1} | x_k)\}_{k=1}^K$  and the weighting/potential functions  $G_K(x_K), \{G_{k-1}(x_k, x_{k-1})\}_{k=1}^K$ . Initially, we draw  $N$  samples from our initial proposal  $x_K^{(i)} \sim M_K = \mathcal{N}(0, I)$  and then weight them according to an initial potential function  $w_K^{(i)} \propto G_K(x_K^{(i)})$ . For  $K$  iterations, we then sequentially propose  $x_{k-1}^{(i)} \sim M_{k-1}(x_{k-1}^{(i)} | x_k^{(i)})$ , weight samples  $w_{k-1}^{(i)} \propto w_k^{(i)} G_{k-1}(x_k^{(i)}, x_{k-1}^{(i)})$ , and resample ([Douc & Cappé, 2005](#)) if our effective sample size (ESS) drops below a certain threshold  $N_{\text{eff}}$ . An overview of this process is given in [Appendix A.1](#). At each iteration  $k$  the SMC algorithm generates a weighted particle population  $\{(x_k^{(i)}, w_k^{(i)})\}_{i=1}^N$  that provides an empirical approximation of the target distribution

$$\begin{aligned} \nu_k(x_{k:K}) &\propto G_K(x_K) M_K(x_K) \\ &\times \prod_{j=k+1}^K G_{j-1}(x_j, x_{j-1}) M_{j-1}(x_{j-1} | x_j). \end{aligned} \quad (9)$$

We apply the SMC framework to sample the posterior distribution in Equation (8) by choosing the proposals and weight functions  $\{M_k, G_k\}_{k=0}^K$  in such a way that the final marginal  $\nu_0(x_0) = p_\theta(x_0 | y)$ . As long as this requirement is fulfilled, the algorithm will provide a consistent (as  $N \rightarrow \infty$ ) Monte Carlo estimate of the target at the final time point regardless of the intermediate marginals. In practice, however, these design choices influence the statistical efficiency of the algorithm (e.g., the weight variance).

## 3. Methodology

### 3.1. PDE Residual Likelihoods

In the context of PDEs, we can express our likelihood as the mean squared error (MSE) of the sparse observations for both  $a$  and  $u$  as well as the PDE equation residuals. That is, we define the *PDE residual likelihood*:

$$\begin{aligned} \log p(y | x) &= -\beta \left( \frac{1}{n} \|u_{\text{obs}} - \mathcal{M}_u \odot x\|_2^2 \right) \\ &\quad - \gamma \left( \frac{1}{n} \|a_{\text{obs}} - \mathcal{M}_a \odot x\|_2^2 \right) \\ &\quad - \omega \left( \frac{1}{m} \|f(c, \tau, x)\|_2^2 \right) + c, \end{aligned} \quad (10)$$

where  $\mathcal{M}_{u,a}$  are the corresponding binary masks indicating the spatial coordinates of the observations,  $n$  is the number of observations,  $m$  is the number of pixels and  $\odot$  is the Hadamard/element-wise product. This likelihood jointly incorporates the governing PDE as a physics constrain, and the sparse observation as a data constrain.

To enable approximate likelihood evaluations at intermediate time steps we follow [Wu et al. \(2023\)](#) and evaluate the

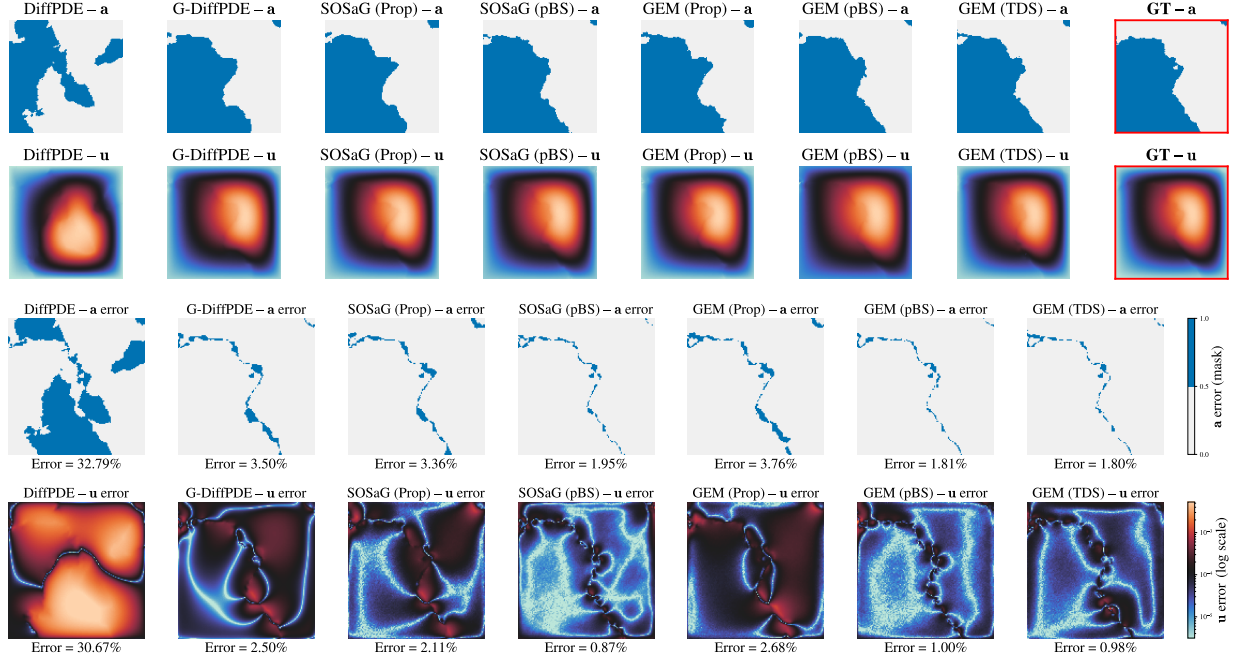


Figure 2. The top two rows show contour plot of the generated PDE solutions and coefficients using different methods. The bottom two rows show the corresponding (relative) error when compared to the ground truth (GT). We especially observe that the most erroneous part are around the edges. This is consistent with the common problem of diffusion models that they tend to smooth out the high-frequency information of the generated samples.

likelihood at reconstructed samples. That is, we define the intermediate approximate likelihood at diffusion time  $t$  as:

$$\begin{aligned} p_t^\theta(y | x_t, \sigma_t) &= \int p(y | x_0) p_\theta(x_0 | x_t) dx_0 \\ &\approx p(y | x_0 = D_\theta(x, \sigma_t)) =: \tilde{p}_\theta(y | x_t), \end{aligned} \quad (11)$$

and as a result, at time 0 we have  $\tilde{p}_\theta(y | x_0) = p(y | x_0)$ .

In the following sections, we show how we can incorporate this likelihood along with different proposals into the SMC framework, by designing suitable  $\{M_k, G_k\}_{k=0}^K$ .

### 3.2. Guided Euler–Maruyama as a Proposal for an SMC Sampler

To numerically sample the SDE (5), a common approximation is the Euler–Maruyama method:

$$x_{k-1} = x_k - (\sigma_{k-1}^2 - \sigma_k^2) \nabla_{x_k} \log p_{k-1}(x_k, \sigma_k) + \sqrt{\sigma_{k-1}^2 - \sigma_k^2} z, \quad (12)$$

where  $z \sim \mathcal{N}(0, I)$ , and the discretization time interval is implicitly accounted in the schedule sequence  $\sigma_k$ . We denote this transition as  $p_\theta(x_{k-1} | x_k) = \mathcal{N}(x_k | \mu_{\text{model}}, (\sigma_{k-1}^2 - \sigma_k^2) I)$ . Using the Euler–Maruyama method to simulate from  $k = K$  to  $k = 0$  we obtain a trajectory distributed according to  $p_\theta(x_{0:K})$ .

If we use the guided score (7) in place of the unconditional score in equation (12), we obtain the guided Euler–Maruyama (GEM) update:

$$\begin{aligned} x_{k-1} &= x_k - (\sigma_{k-1}^2 - \sigma_k^2) \frac{x_k - D_\theta(x_k, \sigma_k)}{\sigma_k^2} \\ &\quad - (\sigma_{k-1}^2 - \sigma_k^2) \nabla_{x_k} \log \tilde{p}_\theta(y | x_k) \\ &\quad + \sqrt{\sigma_{k-1}^2 - \sigma_k^2} z. \end{aligned} \quad (13)$$

Pseudocode for this method is shown in Appendix A.4.1. The GEM update (13) defines a Markov transition kernel  $\tilde{p}_\theta(x_{k-1} | x_k, y) = \mathcal{N}(x_k | \mu_{\text{prop}}, (\sigma_{k-1}^2 - \sigma_k^2) I)$  that can be used as a proposal for SMC. Specifically, we choose the proposal  $M_{k-1}(x_{k-1} | x_k) = \tilde{p}_\theta(x_{k-1} | x_k, y)$ , and the weight update

$$G_{k-1}(x_k, x_{k-1}) = \frac{\tilde{p}_\theta(y | x_{k-1})}{\tilde{p}_\theta(y | x_k)} \frac{p_\theta(x_{k-1} | x_k)}{\tilde{p}_\theta(x_{k-1} | x_k, y)} \quad (14)$$

This was used in the Twisted Diffusion Sampler (TDS, Wu et al., 2023), and we can verify using the FK formula (9) and substituting in our proposal and weight update that, the marginal distribution we target at each iteration is:

$$\begin{aligned} v_{k-1}(x_{k-1:K}) &\propto \tilde{p}_\theta(y | x_{k-1}) p_\theta(x_{k-1:K}) \\ v_{0:K}(x_{0:K}) &= p_\theta(x_{0:K} | y). \end{aligned} \quad (15)$$

### 3.3. Second-Order Stochastic Guided Proposal

Although Euler–Maruyama is common, it is not the most efficient SDE integrator and Karras et al. (2022) propose using 2nd order stochastic sampling process. First, the noise scale is jittered and then the ODE dynamics via the denoiser are run, i.e. we run the following set of equations:

$$\hat{\sigma}_k \leftarrow \sigma_k + \gamma_k \sigma_k, \quad (16)$$

$$\hat{x}_k = x_k + \sqrt{\hat{\sigma}_k^2 - \sigma_k^2} \psi, \quad \psi \sim \mathcal{N}(0, I), \quad (17)$$

$$x_{k-1} = \hat{x}_k + (\sigma_{k-1}^2 - \hat{\sigma}_k^2) \frac{\hat{x}_k - D_\theta(\hat{x}_k, \hat{\sigma}_k)}{\hat{\sigma}_k^2}, \quad (18)$$

where  $\gamma_k$  is a constant used to reach a higher noise level. The full details of this can be found in Karras et al. (2022). Notice how this algorithm adds noise before computing the denoised mean. Including guidance information as outlined previously, (18) becomes:

$$x_{k-1} = \hat{x}_k + (\sigma_{k-1}^2 - \hat{\sigma}_k^2) \frac{\hat{x}_k - D_\theta(\hat{x}_k, \hat{\sigma}_k)}{\hat{\sigma}_k^2} - (\sigma_{k-1}^2 - \hat{\sigma}_k^2) \nabla_{\hat{x}_k} \log \tilde{p}_\theta(y | \hat{x}_k). \quad (19)$$

This method uses a second-order correction method to improve sampling quality. This was also implemented in the DiffusionPDE framework (Huang et al., 2024), albeit with a deterministic (ODE-based) formulation. We also use the 2nd order correction as part of our proposal but, importantly, with the stochastic jittering. We refer to this proposal as the Second-Order Stochastic Guided (SOSaG) proposal.

Although the SOSaG integrator is shown to be empirically powerful, it is not straightforward to incorporate it as the proposal  $M$  in SMC. The reason is that the weight computation in equation (14) requires a point-evaluatable proposal density which is not the case for SOSaG. Clearly, unlike Euler–Maruyama, now  $x_{k-1}$  conditioned on  $x_k$  does not retain the Gaussianity after passing through the non-linear denoiser. However, we can instead work on a new Feynman–Kac model  $\bar{\nu}_{0:K}$  with components defined in a “bootstrap” fashion, which we call psuedo-bootstrap (pBS):

$$\begin{aligned} \bar{M}_{k-1}(x_{k-1} | x_k) &= \bar{p}_\theta(x_{k-1} | x_k, y), \\ \bar{G}_{k-1}(x_k, x_{k-1}) &= \frac{\tilde{p}_\theta(y | x_{k-1})}{\tilde{p}_\theta(y | x_k)}, \end{aligned}$$

where  $\bar{p}_\theta(x_{k-1} | x_k, y)$  denotes the distribution of SOSaG proposal described in equation (19). At the terminal time  $k = 0$ , this new model recovers  $\bar{\nu}_0(x_0) = \bar{p}_\theta(x_0 | y) p_\theta(y | x_0)$ , where  $\bar{p}_\theta(x_0 | y)$  is an approximate posterior distribution obtained by simulating the SOSaG proposal without SMC correction (see Appendix A.3 for the derivation). Although this new target is no longer the same as the original in (15), it is motivated in this PDE context, as we explain in the following.

### 3.4. Bridging between pBS and PINNs

When using the pBS framework, our target distribution is altered so it is multiplied by an extra likelihood factor. Theoretically, we could choose to use any multiple of the likelihood depending on our belief in the diffusion prior and the PDE residual likelihood:

$$\bar{\nu}_{0:K}(x_{0:K}) \propto \bar{p}_\theta(x_0 | y) \tilde{p}_\theta(y | x_0)^\rho, \quad (20)$$

where  $\bar{p}_\theta(x_0 | y)$  is the final marginal of the SOSaG proposal,  $\rho$  is often called the *tempering* parameter (Neal, 2001; Buchholz et al., 2021). In our case, the temperature is simply  $\rho = 1$ . As  $\rho$  increases, the target is dominated by the likelihood which approaches a pure maximum likelihood estimation (MLE) task which is the framework PINNs use. This is essentially changing the precision of the PDE residual likelihood. This also gives us a way to control our prior belief. It is unlikely that our diffusion prior will perfectly model probability distribution of the PDE governing the data. Therefore, a traditional SMC sampling method will approach the desired target, but this target may not be the optimal-in-practice solution to our problem. Empirically, we find that this produces better results and therefore it motivates that the “true target” is different than the one converged upon by Equation (15).

### 3.5. SMC and Evolutionary Algorithms

A common criticism of SMC, especially when sampling from diffusion models is the effective sample size (ESS) degenerates as  $k \rightarrow 0$  (Wu et al., 2023; Corenflos et al., 2025; Zhao, 2026), often only leaving a single particle with a weight that contributes towards the target estimate, despite having relatively high ESS at the beginning. However conversely, it has also largely been empirically shown that SMC samplers still work well albeit the particle coalescence issue. To generate diverse samples, Dou & Song (2024); Trippe et al. (2023) run the SMC independently many times, usually with a low number of particles and keeping a single particle per iteration. This results in a biased, but empirically effective, approximation of the SMC target distribution.

The efficacy of this approach can be understood as a form of evolutionary algorithm (Bäck & Schwefel, 1993; Yu & Gen, 2010), where the weights represent the survival probabilities, the proposal stands for mutation, and the resampling act as a selection function. Evolutionary algorithms are inspired by biological models, and they have been largely shown to work in many machine learning problems (Wang et al., 2024; Novikov et al., 2025). As such, the effectiveness of SMC samplers for diffusion models albeit the *statistical* degeneracy, may still be justified on these grounds.

Table 1. Performance across PDE benchmarks.

Experiment	Method	$a$	$u$	Avg.
DF	DiffPDE-NoG	49.48 <sub>13.71</sub>	33.22 <sub>8.91</sub>	41.35
	DiffPDE	3.47 <sub>0.22</sub>	3.31 <sub>0.91</sub>	3.39
	EM (TDS)	1.86 <sub>0.24</sub>	1.22 <sub>1.22</sub>	1.54
	EM (pBS)	1.85 <sub>0.23</sub>	<b>1.03<sub>0.77</sub></b>	<b>1.44</b>
	SOSaG (N=1)	3.35 <sub>0.29</sub>	2.94 <sub>0.82</sub>	3.15
IHE	SOSaG (pBS)	<b>1.81<sub>0.17</sub></b>	1.15 <sub>0.82</sub>	1.48
	DiffPDE-NoG	159.96 <sub>36.75</sub>	184.85 <sub>62.66</sub>	172.41
	DiffPDE	13.33 <sub>0.47</sub>	16.61 <sub>10.23</sub>	14.97
	EM (TDS)	12.69 <sub>0.42</sub>	2.98 <sub>0.15</sub>	7.84
	EM (pBS)	12.79 <sub>0.39</sub>	<b>2.96<sub>0.17</sub></b>	7.88
BNS	SOSaG (N=1)	13.56 <sub>0.44</sub>	13.90 <sub>7.50</sub>	13.73
	SOSaG (pBS)	<b>12.49<sub>0.37</sub></b>	2.99 <sub>0.18</sub>	<b>7.74</b>
	DiffPDE-NoG	51.04 <sub>19.44</sub>	50.32 <sub>17.64</sub>	50.68
	DiffPDE	2.37 <sub>0.84</sub>	2.83 <sub>0.72</sub>	2.60
	EM (TDS)	2.28 <sub>0.60</sub>	2.36 <sub>0.55</sub>	2.32
NBNS	EM (pBS)	7.97 <sub>0.25</sub>	<b>1.75<sub>0.09</sub></b>	4.86
	SOSaG (N=1)	2.12 <sub>0.67</sub>	2.38 <sub>0.64</sub>	2.25
	SOSaG (pBS)	<b>2.07<sub>0.46</sub></b>	2.29 <sub>0.37</sub>	<b>2.18</b>
	DiffPDE-NoG	158.18 <sub>21.57</sub>	171.63 <sub>26.30</sub>	164.91
	DiffPDE	10.21 <sub>0.47</sub>	5.22 <sub>0.57</sub>	7.72
Poisson	EM (TDS)	7.94 <sub>0.20</sub>	<b>1.74<sub>0.06</sub></b>	4.84
	EM (pBS)	7.97 <sub>0.25</sub>	1.75 <sub>0.09</sub>	4.86
	SOSaG (N=1)	10.34 <sub>0.58</sub>	5.52 <sub>0.66</sub>	7.93
	SOSaG (pBS)	<b>7.81<sub>0.24</sub></b>	<b>1.74<sub>0.07</sub></b>	<b>4.78</b>
	DiffPDE-NoG	156.87 <sub>35.51</sub>	160.97 <sub>52.81</sub>	158.92
Poisson	DiffPDE	11.25 <sub>0.32</sub>	6.72 <sub>3.36</sub>	8.99
	EM (TDS)	10.51 <sub>0.28</sub>	2.14 <sub>0.11</sub>	6.33
	EM (pBS)	10.50 <sub>0.23</sub>	<b>2.13<sub>0.11</sub></b>	6.32
	SOSaG (N=1)	11.34 <sub>0.38</sub>	9.12 <sub>5.12</sub>	10.23
	SOSaG (pBS)	<b>10.40<sub>0.25</sub></b>	2.15 <sub>0.10</sub>	<b>6.28</b>

## 4. Experiments

### 4.1. Benchmark PDEs

We first test our results on five common benchmark PDEs. Darcy flow (DF), inhomogeneous Helmholtz equation (IHE), non-bounded Navier–Stokes (NBNS), bounded Navier–Stokes (BNS) and the Poisson Equation. We have provided further details of these in Appendix B.1.1. Our experimental implementation is based on the open-source code released by Huang et al. (2024), which we adapted and extended for our specific experimental setting. We used the pretrained models they provided. As a baseline, we used the DiffusionPDE sampling method (Huang et al., 2024) with guidance (DiffPDE) and without it (DiffPDE-NoG). DiffPDE is the original algorithm which uses the guidance information during sampling, DiffPDE-NoG forgoes this guidance information and as such is a purely data driven approach to solving the PDEs. We restricted our comparison to this as the original DiffPDE significantly outperformed other baselines such as PINNs, Deep-ONets, PINOs and FNOs; see Huang et al. (2024, Section 4).

We compare the baselines against three configurations of

our SMC method, each using  $N = 8$  particles and the proposal variant of SOSaG which is the equivalent of  $N = 1$  in an SMC framework. Note that this is similar to DiffPDE but with stochastic instead of deterministic sampling. We use the GEM proposal with both the TDS and the pBS framework, while the SOSaG proposal requires the pBS weighting. For both  $u$  and  $a$  our sparse observations consist of 500 pixels for each experiment. Figure 1 gives examples of these observations. The PDE snapshots each have  $128 \times 128$  spatial grids which means we only observe  $\approx 3.05\%$  of the PDE data information. All results were averaged over 100 independent runs.

### 4.2. Multiphysics PDE Systems with Observation Noise

Next, we test the methods on a multiphysics system of interacting PDEs. For this we chose a 2-species and 3-species Reaction-Diffusion (Kondo & Miura, 2010; Britton, 1986) (2SRD and 3SRD respectively), where with 2SRD we have to estimate the two scalar fields and two coefficient fields, one for each interacting PDE. For the 3SRD experiment, we aim to recover a solution field ( $u, v, z$ ) and coefficient field ( $D_u, D_v, D_z$ ) associated with each interacting PDE. We have provided more details of this in Appendix B.1.2. We also tested both examples with varying levels of noise  $\sigma_O$  added to the observations in order to test the ability of the sampling methods under potentially more realistic scenarios, where the observations may not be perfectly aligned with the underlying equations.

It was found that the low ESS of both the EM pBS and the EM TDS variant caused the same set of particles to be resampled and therefore the performance was identical for the same random seed. Therefore we have only reported the results of the pBS variant, as it requires less model evaluations than the TDS variant. Our stochastic sampling methods also use  $N = 4$  samples for these experiments as the larger systems of equations have an increased memory overhead.

## 5. Discussion

Table 1 shows the results across the PDE benchmarks. The tables give the relative error in percent compared to the error calculated by finite element methods (FEMs) which are used to generate the data and therefore we assume to be the ground truth, with the standard deviation given in the subscript. DiffPDE outperforms DiffPDE-NoG by a large margin. This is expected as the DiffPDE-NoG approach is a purely data driven method, therefore this shows that the guidance information is essential when solving complex PDEs. We notice that the SMC algorithms consistently outperform the baselines in both the estimation of  $u$  and  $a$ , despite having a low ESS. In particular, the SOSaG proposal getting the best  $a$  estimates and generally EM-pBS getting

Table 2. Performance across methods on the 2SRD and 3SRD experiments for varying observation noise levels  $\sigma_O$ .

Method	2SRD (2 species)					3SRD (3 species)						
	$D_u$	$D_v$	$u$	$v$	Avg.	$D_u$	$D_v$	$D_z$	$u$	$v$	$z$	Avg.
$\sigma_O = 0.0$												
DiffPDE-NoG	47.34 <sub>8.91</sub>	62.44 <sub>8.81</sub>	0.19 <sub>0.05</sub>	19.78 <sub>8.30</sub>	32.44 <sub>3.25</sub>	57.33 <sub>6.39</sub>	67.64 <sub>11.89</sub>	72.17 <sub>13.45</sub>	3.43 <sub>0.65</sub>	8.10 <sub>1.53</sub>	5.10 <sub>1.57</sub>	35.63 <sub>3.09</sub>
DiffPDE	3.67 <sub>0.04</sub>	<b>2.93<sub>0.07</sub></b>	0.18 <sub>0.03</sub>	13.57 <sub>3.82</sub>	5.09 <sub>0.95</sub>	8.83 <sub>0.08</sub>	<b>6.64<sub>0.23</sub></b>	22.13 <sub>0.11</sub>	3.64 <sub>0.24</sub>	7.08 <sub>0.89</sub>	4.04 <sub>0.83</sub>	8.73 <sub>0.18</sub>
EM (pBS)	<b>3.64<sub>0.06</sub></b>	3.10 <sub>0.09</sub>	<b>0.03<sub>0.01</sub></b>	<b>1.35<sub>0.06</sub></b>	<b>2.03<sub>0.03</sub></b>	<b>8.72<sub>0.09</sub></b>	6.93 <sub>0.21</sub>	21.99 <sub>0.16</sub>	<b>0.09<sub>0.01</sub></b>	<b>0.34<sub>0.04</sub></b>	<b>0.37<sub>0.03</sub></b>	<b>6.41<sub>0.05</sub></b>
SOSaG (pBS)	3.67 <sub>0.09</sub>	3.12 <sub>0.10</sub>	<b>0.03<sub>0.01</sub></b>	<b>1.35<sub>0.05</sub></b>	2.04 <sub>0.04</sub>	8.73 <sub>0.14</sub>	6.85 <sub>0.20</sub>	<b>21.97<sub>0.11</sub></b>	0.09 <sub>0.01</sub>	0.40 <sub>0.03</sub>	0.39 <sub>0.03</sub>	<b>6.41<sub>0.04</sub></b>
$\sigma_O = 0.005$												
DiffPDE-NoG	47.34 <sub>8.91</sub>	62.44 <sub>8.81</sub>	0.19 <sub>0.05</sub>	19.78 <sub>8.30</sub>	32.44 <sub>3.25</sub>	57.33 <sub>6.39</sub>	67.64 <sub>11.89</sub>	72.17 <sub>13.45</sub>	3.43 <sub>0.65</sub>	8.10 <sub>1.53</sub>	5.10 <sub>1.57</sub>	35.63 <sub>3.09</sub>
DiffPDE	4.58 <sub>0.12</sub>	4.79 <sub>0.19</sub>	0.17 <sub>0.03</sub>	13.77 <sub>3.85</sub>	5.82 <sub>0.95</sub>	9.27 <sub>0.06</sub>	7.85 <sub>0.18</sub>	22.51 <sub>0.09</sub>	3.54 <sub>0.25</sub>	7.25 <sub>0.89</sub>	4.06 <sub>0.84</sub>	9.08 <sub>0.18</sub>
EM (pBS)	4.62 <sub>0.17</sub>	4.46 <sub>0.09</sub>	0.11 <sub>0.01</sub>	7.01 <sub>0.53</sub>	4.05 <sub>0.15</sub>	9.06 <sub>0.14</sub>	<b>7.79<sub>0.25</sub></b>	22.24 <sub>0.16</sub>	0.14 <sub>0.02</sub>	<b>0.54<sub>0.06</sub></b>	<b>0.70<sub>0.06</sub></b>	<b>6.74<sub>0.06</sub></b>
SOSaG (pBS)	<b>4.56<sub>0.18</sub></b>	<b>4.44<sub>0.10</sub></b>	<b>0.10<sub>0.01</sub></b>	<b>6.27<sub>0.67</sub></b>	<b>3.84<sub>0.18</sub></b>	<b>9.05<sub>0.15</sub></b>	7.86 <sub>0.29</sub>	<b>22.15<sub>0.20</sub></b>	<b>0.13<sub>0.02</sub></b>	0.66 <sub>0.09</sub>	<b>0.70<sub>0.10</sub></b>	6.76 <sub>0.07</sub>
$\sigma_O = 0.01$												
DiffPDE-NoG	47.34 <sub>8.91</sub>	62.44 <sub>8.81</sub>	0.19 <sub>0.05</sub>	19.78 <sub>8.30</sub>	32.44 <sub>3.25</sub>	57.33 <sub>6.39</sub>	67.64 <sub>11.89</sub>	72.17 <sub>13.45</sub>	3.43 <sub>0.65</sub>	8.10 <sub>1.53</sub>	5.10 <sub>1.57</sub>	35.63 <sub>3.09</sub>
DiffPDE	5.87 <sub>0.26</sub>	7.00 <sub>0.30</sub>	0.16 <sub>0.03</sub>	13.56 <sub>3.76</sub>	6.65 <sub>0.92</sub>	10.13 <sub>0.08</sub>	9.83 <sub>0.17</sub>	23.29 <sub>0.09</sub>	3.44 <sub>0.27</sub>	7.38 <sub>0.90</sub>	4.14 <sub>0.87</sub>	9.70 <sub>0.18</sub>
EM (pBS)	5.73 <sub>0.18</sub>	<b>6.21<sub>0.19</sub></b>	0.15 <sub>0.01</sub>	10.39 <sub>1.18</sub>	5.62 <sub>0.29</sub>	10.01 <sub>0.18</sub>	10.09 <sub>0.56</sub>	23.37 <sub>0.32</sub>	0.21 <sub>0.07</sub>	1.23 <sub>0.24</sub>	<b>0.93<sub>0.15</sub></b>	7.64 <sub>0.20</sub>
SOSaG (pBS)	<b>5.71<sub>0.18</sub></b>	6.23 <sub>0.15</sub>	<b>0.13<sub>0.01</sub></b>	<b>8.37<sub>0.80</sub></b>	<b>5.12<sub>0.19</sub></b>	<b>9.77<sub>0.14</sub></b>	<b>9.50<sub>0.36</sub></b>	<b>22.84<sub>0.27</sub></b>	<b>0.16<sub>0.03</sub></b>	<b>0.98<sub>0.19</sub></b>	0.96 <sub>0.16</sub>	<b>7.37<sub>0.12</sub></b>
$\sigma_O = 0.02$												
DiffPDE-NoG	47.34 <sub>8.91</sub>	62.44 <sub>8.81</sub>	0.19 <sub>0.05</sub>	19.78 <sub>8.30</sub>	32.44 <sub>3.25</sub>	57.33 <sub>6.39</sub>	67.64 <sub>11.89</sub>	72.17 <sub>13.45</sub>	3.43 <sub>0.65</sub>	8.10 <sub>1.53</sub>	5.10 <sub>1.57</sub>	35.63 <sub>3.09</sub>
DiffPDE	8.24 <sub>0.33</sub>	10.73 <sub>0.25</sub>	<b>0.16<sub>0.03</sub></b>	13.40 <sub>3.82</sub>	8.13 <sub>0.94</sub>	12.30 <sub>0.13</sub>	14.08 <sub>0.28</sub>	25.18 <sub>0.13</sub>	3.34 <sub>0.31</sub>	7.51 <sub>0.94</sub>	4.24 <sub>0.92</sub>	11.11 <sub>0.22</sub>
EM (pBS)	8.14 <sub>0.63</sub>	<b>9.69<sub>0.36</sub></b>	0.21 <sub>0.01</sub>	16.48 <sub>1.74</sub>	8.63 <sub>0.46</sub>	11.71 <sub>0.14</sub>	14.54 <sub>0.48</sub>	25.92 <sub>0.31</sub>	0.59 <sub>0.07</sub>	2.38 <sub>0.25</sub>	1.70 <sub>0.21</sub>	9.47 <sub>0.14</sub>
SOSaG (pBS)	<b>7.98<sub>0.36</sub></b>	9.88 <sub>0.35</sub>	0.18 <sub>0.01</sub>	<b>13.11<sub>1.11</sub></b>	<b>7.79<sub>0.21</sub></b>	<b>11.58<sub>0.20</sub></b>	<b>13.59<sub>0.55</sub></b>	<b>25.07<sub>0.47</sub></b>	<b>0.35<sub>0.11</sub></b>	<b>1.89<sub>0.38</sub></b>	<b>1.54<sub>0.23</sub></b>	<b>9.00<sub>0.24</sub></b>

the best  $u$  estimate, and based on the average error SOSaG performs the best. Figure 2 shows the reconstructed fields and the relative errors for a single run for the DF experiment. We can see that the relative error is visually lower for the SMC methods. We have provided single run plots for all experiments in Appendix C.

Table 2 shows the results for the 2SRD and 3SRD experiments. We can see that the performance degrades as the observation noise increases, an intuitive result. However, across nearly all results, the stochastic methods outperform the ODE ones. We also see that under higher noise levels, the SOSaG proposal tends to outperform the EM proposal. We hypothesize that under noisy observations, the second order correction present in the SOSaG proposal helps account for this and therefore produces superior results which may lead to it being a better choice of sampling method in real-world scenarios.

Despite the DiffPDE method occasionally producing better results for some of the relative errors associated with the coefficient fields, they under-perform when trying to approximate the solution fields. Although the relative error is low, the scalar fields seem to be sensitive even to small errors. The recon and error plots provided in Appendix C demonstrate this visually. Despite the low errors on the scalar fields, we can see that the reconstructed field does not well represent the ground truth. The stochastic methods on the other hand approximate this field much better.

## 6. Limitations and Further Work

Appendix C shows our methods incur an increased time cost compared to the baseline as the number of samples increases. An optimal implementation would limit the extra wall clock time needed. The score model we call sequentially gets the score for each sample. This can be vectorized and will instantly speed up the algorithm.

In Appendix C table 5 gives an ablation study for varying sample sizes when using the SMC framework. We note that increasing the number of samples reduces the error in the estimates, a result which is corroborated by the wider Monte Carlo literature (Chopin, 2004; Meyn & Tweedie, 2012; Robert et al., 1999). Due to the size of the flow fields/system states generated, the limit for the GPU we used was 8 samples on the smaller experiments and 4 on the larger ones. This motivates the development of a multi-GPU implementation of an SMC sampler to refine PDE estimates.

The PDE residual intermediate likelihoods (and their gradients) can be computationally demanding to evaluate, especially for high-order and large PDE systems. It would be interesting to explore numerical acceleration techniques for the likelihood computation, and incorporate it within the SMC framework as an (possibly unbiased) estimation of the potential function. Another direction might be assuming a pre-trained PINN and use it as a distilled surrogate for computing the intermediate likelihoods.

## Acknowledgment

This work was partially supported by the Swedish Research Council (project no: 2024-05011), the Wallenberg AI, Autonomous Systems and Software Program (WASP) funded by the Knut and Alice Wallenberg (KAW) Foundation, and the Excellence Center at Linköping–Lund in Information Technology (ELLIIT). Computations were enabled by the supercomputing resource Berzelius provided by National Supercomputer Centre at Linköping University and the KAW foundation.

## Impact Statement

This paper presents work whose goal is to advance the field of Machine Learning. There are many potential societal consequences of our work, none which we feel must be specifically highlighted here.

## References

Albergo, M., Boffi, N. M., and Vanden-Eijnden, E. Stochastic Interpolants: A Unifying Framework for Flows and Diffusions. *Journal of Machine Learning Research*, 26(209):1–80, 2025. URL <http://jmlr.org/papers/v26/23-1605.html>.

Ames, W. F. *Nonlinear Partial Differential Equations in Engineering: Mathematics in Science and Engineering: A Series of Monographs and Textbooks*, volume 18. Elsevier, 2016.

Bäck, T. and Schwefel, H.-P. An Overview of Evolutionary Algorithms for Parameter Optimization. *Evolutionary Computation*, 1(1):1–23, 1993.

Barati Farimani, A., Gomes, J., and Pande, V. Deep Learning the Physics of Transport Phenomena. *arXiv preprint arXiv:1709.02432*, 09 2017. doi: 10.48550/arXiv.1709.02432.

Britton, N. *Reaction-diffusion equations and their applications to biology*. Elsevier Academic Press Inc, USA United States, 1986.

Buchholz, A., Chopin, N., and Jacob, P. E. Adaptive Tuning of Hamiltonian Monte Carlo within Sequential Monte Carlo. *Bayesian Analysis*, 16(3):745–771, 2021.

Cai, S., Mao, Z., Wang, Z., Yin, M., and Karniadakis, G. E. Physics-Informed Neural Networks (PINNs) for Fluid Mechanics: A Review. *Acta Mechanica Sinica*, 37(12): 1727–1738, 2021a.

Cai, S., Wang, Z., Wang, S., Perdikaris, P., and Karniadakis, G. E. Physics-Informed Neural Networks for Heat Transfer Problems. *Journal of Heat Transfer*, 143(6):060801, 2021b.

Cao, H., Tan, C., Gao, Z., Xu, Y., Chen, G., Heng, P.-A., and Li, S. Z. A Survey on Generative Diffusion Models. *IEEE Transactions on Knowledge and Data Engineering*, 36(7):2814–2830, 2024.

Cardoso, G., el idrissi, Y. J., Corff, S. L., and Moulines, E. Monte Carlo guided Denoising Diffusion models for Bayesian linear inverse problems. In *The Twelfth International Conference on Learning Representations*, 2024. URL <https://openreview.net/forum?id=nHESwXvxWK>.

Chopin, N. Central Limit Theorem for Sequential Monte Carlo Methods and Its Application to Bayesian Inference. *The Annals of Statistics*, 32(6):2385–2411, 2004. doi: 10.1214/009053604000000698. URL <https://doi.org/10.1214/009053604000000698>.

Chopin, N., Papaspiliopoulos, O., et al. *An Introduction to Sequential Monte Carlo*, volume 4. Springer, 2020.

Chung, H., Kim, J., and Ye, J. C. Diffusion models for inverse problems, 2025. URL <https://arxiv.org/abs/2508.01975>.

Corenflos, A., Zhao, Z., Särkkä, S., Sjölund, J., and Schön, T. B. Conditioning diffusion models by explicit forward-backward bridging. In *Proceedings of the 28th International Conference on Artificial Intelligence and Statistics (AISTATS)*, volume 258, pp. 3709–3717. PMLR, 2025.

Crank, J. and Nicolson, P. A Practical Method for Numerical Evaluation of Solutions of Partial Differential Equations of the Heat-Conduction Type. In *Mathematical Proceedings of the Cambridge Philosophical Society*, volume 43, pp. 50–67. Cambridge University Press, 1947.

Creswell, A., White, T., Dumoulin, V., Arulkumaran, K., Sengupta, B., and Bharath, A. A. Generative Adversarial Networks: An Overview. *IEEE Signal Processing Magazine*, 35(1):53–65, 2018.

Dang, M., Han, J., Xu, M., Xu, K., Srivastava, A., and Ermon, S. Inference-time scaling of diffusion language models with particle Gibbs sampling. *arXiv preprint arXiv:2507.08390*, 2025.

Dasar, G., Chung, H., Lai, C.-H., Mitsufuji, Y., Ye, J. C., Milanfar, P., Dimakis, A. G., and Delbracio, M. A Survey on Diffusion Models for Inverse Problems, 2024. URL <https://arxiv.org/abs/2410.00083>.

Dhariwal, P. and Nichol, A. Diffusion Models Beat GANs on Image Synthesis. *Advances in Neural Information Processing Systems*, 34:8780–8794, 2021.

Dou, Z. and Song, Y. Diffusion Posterior Sampling for Linear Inverse Problem Solving: A Filtering Perspective.

In *The Twelfth International Conference on Learning Representations*, 2024.

Douc, R. and Cappé, O. Comparison of Resampling Schemes for Particle Filtering. In *ISPA 2005. Proceedings of the 4th International Symposium on Image and Signal Processing and Analysis*, 2005., pp. 64–69. IEEE, 2005.

Eason, J. and Cremaschi, S. Adaptive Sequential Sampling for Surrogate Model Generation with Artificial Neural Networks. *Computers & Chemical Engineering*, 68:220–232, 2014.

Evans, L. C. *Partial Differential Equations*, volume 19. American Mathematical Society, 2022.

Gonzalez, F. J. and Balajewicz, M. Deep Convolutional Recurrent Autoencoders for Learning Low-Dimensional Feature Dynamics of Fluid Systems. *arXiv preprint arXiv:1808.01346*, 2018.

Guo, Z., Liu, J., Wang, Y., Chen, M., Wang, D., Xu, D., and Cheng, J. Diffusion Models in Bioinformatics and Computational Biology. *Nature Reviews Bioengineering*, 2(2):136–154, 2024.

Ho, J., Jain, A., and Abbeel, P. Denoising Diffusion Probabilistic Models. *Advances in Neural Information Processing Systems*, 33:6840–6851, 2020.

Huang, J., Yang, G., Wang, Z., and Park, J. J. Diffusion-PDE: Generative PDE-Solving under Partial Observation, 2024. URL <https://openreview.net/forum?id=z0I2SbjN0R>.

Huang, R., Huang, J., Yang, D., Ren, Y., Liu, L., Li, M., Ye, Z., Liu, J., Yin, X., and Zhao, Z. Make-an-Audio: Text-to-Audio Generation with Prompt-Enhanced Diffusion Models. In *International Conference on Machine Learning*, pp. 13916–13932. PMLR, 2023.

Janati, Y., Moufad, B., Abou El Qassime, M., Durmus, A. O., Moulines, E., and Olsson, J. A mixture-based framework for guiding diffusion models. In *Proceedings of the 42nd International Conference on Machine Learning (ICML)*, 2025. URL <https://openreview.net/forum?id=HIOA3bScFB>.

Johnson, C. *Numerical Solution of Partial Differential Equations by the Finite Element Method*. Courier Corporation, 2009.

Kalaivanan, A., Zhao, Z., Sjölund, J., and Lindsten, F. ESS-Flow: Training-free guidance of flow-based models as inference in source space. *arXiv preprint arXiv:2510.05849*, 2025.

Karras, T., Aittala, M., Aila, T., and Laine, S. Elucidating the Design Space of Diffusion-Based Generative Models, 2022. URL <https://openreview.net/forum?id=k7FuTOWMoC7>.

Kelvinius, F. E., Zhao, Z., and Lindsten, F. Solving Linear-Gaussian Bayesian Inverse Problems with Decoupled Diffusion Sequential Monte Carlo. In *Proceedings of the 42nd International Conference on Machine Learning*, volume 267 of *Proceedings of Machine Learning Research*, pp. 15148–15181. PMLR, 13–19 Jul 2025.

Kochkov, D., Smith, J. A., Alieva, A., Wang, Q., Brenner, M. P., and Hoyer, S. Machine learning–accelerated computational fluid dynamics. *Proceedings of the National Academy of Sciences*, 118(21), 2021.

Kohl, G., Chen, L., and Thuerey, N. Benchmarking Autoregressive Conditional Diffusion Models for Turbulent Flow Simulation. In *ICML 2024 AI for Science Workshop*, 2024. URL <https://openreview.net/forum?id=5EdFkEmjr3>.

Kondo, S. and Miura, T. Reaction-Diffusion Model as a Framework for Understanding Biological Pattern Formation. *Science*, 329(5999):1616–1620, 2010. doi: 10.1126/science.1179047. URL <https://www.science.org/doi/10.1126/science.1179047>.

Kong, Z., Ping, W., Huang, J., Zhao, K., and Catanzaro, B. DiffWave: A Versatile Diffusion Model for Audio Synthesis. In *International Conference on Learning Representations*, 2021. URL <https://openreview.net/forum?id=a-xFK8Ymz5J>.

LeVeque, R. J. *Finite Difference Methods for Ordinary and Partial Differential Equations: Steady-State and Time-Dependent Problems*. SIAM, 2007.

Li, Z., Kovachki, N. B., Azizzadenesheli, K., Liu, B., Bhattacharya, K., Stuart, A., and Anandkumar, A. Fourier Neural Operator for Parametric Partial Differential Equations. In *International Conference on Learning Representations*, 2021. URL <https://openreview.net/forum?id=c8P9NQVtmn0>.

Li, Z., Huang, D. Z., Liu, B., and Anandkumar, A. Fourier Neural Operator with Learned Deformations for PDEs on General Geometries. *Journal of Machine Learning Research*, 24(388):1–26, 2023.

Li, Z., Zhou, A. Y., and Farimani, A. B. Generative Latent Neural PDE Solver using Flow Matching. *CoRR*, abs/2503.22600, March 2025. URL <https://doi.org/10.48550/arXiv.2503.22600>.

Lienen, M., Lüdke, D., Hansen-Palmus, J., and Günemann, S. From Zero to Turbulence: Generative Modeling for 3D Flow Simulation. In *The Twelfth International Conference on Learning Representations*, 2024. URL <https://openreview.net/forum?id=ZhlwoC1XaN>.

Lipman, Y., Chen, R. T. Q., Ben-Hamu, H., Nickel, M., and Le, M. Flow Matching for Generative Modeling. In *The Eleventh International Conference on Learning Representations*, 2023. URL <https://openreview.net/forum?id=PqvMRDCJ9t>.

Liu, H., Chen, Z., Yuan, Y., Mei, X., Liu, X., Mandic, D. P., Wang, W., and Plumbley, M. D. AudioLDM: Text-to-Audio Generation with Latent Diffusion Models. In *ICML*, pp. 21450–21474, 2023. URL <https://proceedings.mlr.press/v202/liu23f.html>.

Liu, Q. and Thuerey, N. Uncertainty-Aware Surrogate Models for Airfoil Flow Simulations with Denoising Diffusion Probabilistic Models. *AIAA Journal*, 62(8):2912–2933, 2024. doi: 10.2514/1.J063440. URL <https://doi.org/10.2514/1.J063440>.

Lu, L., Jin, P., and Karniadakis, G. E. DeepONet: Learning Nonlinear Operators for Identifying Differential Equations Based on the Universal Approximation Theorem of Operators. *arXiv preprint arXiv:1910.03193*, 2019.

Lu, L., Jin, P., Pang, G., Zhang, Z., and Karniadakis, G. E. Learning Nonlinear Operators via DeepONet Based on the Universal Approximation Theorem of Operators. *Nature Machine Intelligence*, 3(3):218–229, 2021.

Maxwell, J. C. VIII. A Dynamical Theory of the Electromagnetic Field. *Philosophical Transactions of the Royal Society of London*, 155:459–512, 1865.

Meyn, S. P. and Tweedie, R. L. *Markov Chains and Stochastic Stability*. Springer Science & Business Media, 2012.

Mirza, M. and Osindero, S. Conditional Generative Adversarial Nets. *arXiv preprint arXiv:1411.1784*, 2014.

Molinaro, R., Lanthaler, S., Raonić, B., Rohner, T., Arme-gioiu, V., Simonis, S., Grund, D., Ramic, Y., Wan, Z. Y., Sha, F., et al. Generative AI for Fast and Accurate Statistical Computation of Fluids. *arXiv preprint arXiv:2409.18359*, 2024.

Naesseth, C. A., Lindsten, F., and Schön, T. B. Elements of sequential Monte Carlo. *Foundations and Trends in Machine Learning*, 12(3):307–392, 2019. doi: 10.1561/2200000074. URL <https://arxiv.org/abs/1903.04797>.

Naz, R., Mahomed, F. M., and Mason, D. P. Comparison of Different Approaches to Conservation Laws for Some Partial Differential Equations in Fluid Mechanics. *Applied Mathematics and Computation*, 205(1):212–230, 2008.

Neal, R. M. Annealed Importance Sampling. *Statistics and Computing*, 11(2):125–139, 2001.

Novikov, A., Vũ, N., Eisenberger, M., Dupont, E., Huang, P.-S., Wagner, A. Z., Shirobokov, S., Kozlovskii, B., Ruiz, F. J. R., Mehrabian, A., Kumar, M. P., See, A., Chaudhuri, S., Holland, G., Davies, A., Nowozin, S., Kohli, P., and Balog, M. AlphaEvolve: A coding agent for scientific and algorithmic discovery, 2025. URL <https://arxiv.org/abs/2506.13131>.

Price, I., Sanchez-Gonzalez, A., Alet, F., Andersson, T. R., El-Kadi, A., Masters, D., Ewalds, T., Stott, J., Mohamed, S., Battaglia, P., Lam, R., and Willson, M. Probabilistic Weather Forecasting with Machine Learning. *Nature*, 637:84–90, January 2025. doi: 10.1038/s41586-024-08252-9. URL <https://doi.org/10.1038/s41586-024-08252-9>.

Raissi, M., Perdikaris, P., and Karniadakis, G. E. Physics-Informed Neural Networks: A Deep Learning Framework for Solving Forward and Inverse Problems Involving Nonlinear Partial Differential Equations. *Journal of Computational Physics*, 378:686–707, 2019.

Robert, C. P., Casella, G., and Casella, G. *Monte Carlo Statistical Methods*, volume 2. Springer, 1999.

Rombach, R., Blattmann, A., Lorenz, D., Esser, P., and Ommer, B. High-Resolution Image Synthesis with Latent Diffusion Models. In *Proceedings of the IEEE/CVF Conference on Computer Vision and Pattern Recognition*, pp. 10684–10695, 2022.

Ronneberger, O., Fischer, P., and Brox, T. U-Net: Convolutional Networks for Biomedical Image Segmentation. In *International Conference on Medical Image Computing and Computer-Assisted Intervention*, pp. 234–241. Springer, 2015.

Rozet, F. and Louppe, G. Score-Based Data Assimilation. *Advances in Neural Information Processing Systems*, 36: 40521–40541, 2023.

Sanchez-Gonzalez, A., Godwin, J., Pfaff, T., Ying, R., Leskovec, J., and Battaglia, P. Learning to simulate complex physics with graph networks. In Daumé III, H. and Singh, A. (eds.), *Proceedings of the 37th International Conference on Machine Learning*, volume 119 of *Proceedings of Machine Learning Research*, pp. 8459–8468. PMLR, July

2020. URL <https://proceedings.mlr.press/v119/sanchez-gonzalez20a.html>.

Shysheya, A., Diaconu, C., Bergamin, F., Perdikaris, P., Hernández-Lobato, J. M., Turner, R. E., and Mathieu, E. On conditional diffusion models for PDE simulations. In *Advances in Neural Information Processing Systems 37 (NeurIPS)*, 2024. URL <https://openreview.net/forum?id=nQl8EjyMzh>.

Smith, B. F. *Domain Decomposition Algorithms for the Partial Differential Equations of Linear Elasticity*. New York University, 1990.

Sohl-Dickstein, J., Weiss, E., Maheswaranathan, N., and Ganguli, S. Deep Unsupervised Learning Using Nonequilibrium Thermodynamics. In *International Conference on Machine Learning*, pp. 2256–2265. PMLR, 2015.

Song, Y., Sohl-Dickstein, J., Kingma, D. P., Kumar, A., Ermon, S., and Poole, B. Score-Based Generative Modeling through Stochastic Differential Equations, 2021. URL <https://openreview.net/forum?id=PxTIG12RRHS>.

Stevens, T. S., Nolan, O., Robert, J.-L., and Van Slooten, R. J. Sequential Posterior Sampling with Diffusion Models. In *ICASSP 2025–2025 IEEE International Conference on Acoustics, Speech and Signal Processing (ICASSP)*, pp. 1–5. IEEE, 2025.

Strauss, W. A. *Partial Differential Equations: An Introduction*. John Wiley & Sons, 2007.

Trefethen, L. N. *Spectral Methods in MATLAB*. SIAM, 2000.

Tripathy, R. K. and Bilionis, I. Deep UQ: Learning Deep Neural Network Surrogate Models for High Dimensional Uncertainty Quantification. *Journal of Computational Physics*, 375:565–588, 2018.

Trippé, B. L., Yim, J., Tischer, D., Baker, D., Broderick, T., Barzilay, R., and Jaakkola, T. S. Diffusion Probabilistic Modeling of Protein Backbones in 3D for the motif-scaffolding problem. In *The Eleventh International Conference on Learning Representations*, 2023.

Wang, Y., Zhang, Q., Wang, G.-G., and Cheng, H. The application of evolutionary computation in generative adversarial networks (GANs): a systematic literature survey. *Artificial Intelligence Review*, 57, 06 2024. doi: 10.1007/s10462-024-10818-y.

White, D. A., Arrighi, W. J., Kudo, J., and Watts, S. E. Multiscale Topology Optimization Using Neural Network Surrogate Models. *Computer Methods in Applied Mechanics and Engineering*, 346:1118–1135, 2019.

Wu, L., Trippe, B. L., Naesseth, C. A., Blei, D., and Cunningham, J. P. Practical and asymptotically exact conditional sampling in diffusion models. In *Advances in Neural Information Processing Systems 36 (NeurIPS)*, 2023. URL <https://openreview.net/forum?id=eWKqr1zcRv>.

Yang, G. and Sommer, S. A Denoising Diffusion Model for Fluid Field Prediction. *arXiv preprint arXiv:2301.11661*, 2023.

Yim, J., Stärk, H., Corso, G., Jing, B., Barzilay, R., and Jaakkola, T. S. Diffusion Models in Protein Structure and Docking. *Wiley Interdisciplinary Reviews: Computational Molecular Science*, 14(2):e1711, 2024.

Yu, X. and Gen, M. *Introduction to Evolutionary Algorithms*. Springer, 2010.

Zachmanoglou, E. C. and Thoe, D. W. *Introduction to Partial Differential Equations with Applications*. Courier Corporation, 1986.

Zhao, Z. Generative diffusion posterior sampling for informative likelihoods. *Communications in Information and Systems*, 26(1):151–167, 2026. Special issue for celebrating Thomas Kailath’s 90th birthday.

Zhao, Z., Luo, Z., Sjölund, J., and Schön, T. Conditional sampling within generative diffusion models. *Philosophical Transactions A*, 383(2299):20240329, 2025.

## A. Sequential Monte Carlo Derivations

### A.1. Sequential Monte Carlo Pseudocode

---

**Algorithm 1** Sequential Monte Carlo (SMC)

---

**Require:** Number of particles  $N$ , time steps  $K$ ; proposals  $M_K(x_K), M_k(x_{k-1} \mid x_k)$ ; incremental weight functions  $G_K(x_K), G_k(x_{k-1}, x_k)$ ; resampling threshold  $N_{eff} \in (0, 1]$ .

- 1: **Initialization:**
- 2: **for**  $n = 1 \rightarrow N$  **do**
- 3:    $x_K^{(i)} \sim M_K(x_K)$
- 4:    $w_K^{(i)} = G_K(x_K^{(i)})$
- 5: **end for**
- 6: **for**  $k = K \rightarrow 1$  **do**
- 7:   **for**  $i = 1 \rightarrow N$  **do**
- 8:     **Propagate:**  $x_{k-1}^{(i)} \sim M_k(x_{k-1}^{(i)} \mid x_k^{(i)})$
- 9:     **Weight update:**  $\tilde{w}_{k-1}^{(i)} = w_k^{(i)} G_k(x_{k-1}^{(i)}, x_k^{(i)})$
- 10:   **end for**
- 11:   **Normalize:**  $w_{k-1}^{(i)} = \tilde{w}_{k-1}^{(i)} / \sum_{j=1}^N \tilde{w}_{k-1}^{(j)}$ , for all  $i$
- 12:   **Compute effective sample size:**  $ESS_k = \frac{1}{\sum_{i=1}^N (w_{k-1}^{(i)})^2}$
- 13:   **if**  $ESS_k \leq \tau$  **then**
- 14:     **Resampling (Multinomial):**
- 15:     **for**  $i = 1 \rightarrow N$  **do**
- 16:        $a^{(i)} \sim \text{Cat}(w_{k-1}^{(1)}, \dots, w_{k-1}^{(N)})$
- 17:        $x_{k-1}^{(i)} = x_{k-1}^{(a^{(i)})}$
- 18:        $w_{k-1}^{(i)} = \frac{1}{N}$
- 19:     **end for**
- 20:   **end if**
- 21: **end for**
- 22: **Return:**  $\{(x_0^{(i)}, w_0^{(i)})\}_{i=1}^N$

---

### A.2. EM Proposal

The FK formulation used to derive the targets is provided in equation 9 but we have restated it here for convenience purposes.

$$\nu(x_{0:K}) = \frac{1}{\mathcal{L}} G_K(x_K) M_K(x_K) \prod_{j=1}^k G_{j-1}(x_j, x_{j-1}) M_{j-1}(x_{j-1} \mid x_j) \quad (21)$$

Where  $\mathcal{L}$  is the normalisation constant. Using

$$\begin{aligned} M_K(x_K) &= p_K(x_K), & M_{j-1}(x_{j-1} \mid x_j) &= \tilde{p}_\theta(x_{j-1} \mid x_j, y), \\ G_K(x_K) &= \tilde{p}_\theta(y \mid x_K), & G_{j-1}(x_j, x_{j-1}) &= \frac{\tilde{p}_\theta(y \mid x_{j-1})}{\tilde{p}_\theta(y \mid x_j)} \frac{p_\theta(x_{j-1} \mid x_k)}{\tilde{p}_\theta(x_{j-1} \mid x_j, y)}. \end{aligned}$$

Substituting these into equation 21:

$$\nu(x_{s:K}) \propto \tilde{p}_\theta(y \mid x_K) p_K(x_K) \prod_{j=s}^k \frac{\tilde{p}_\theta(y \mid x_{j-1})}{\tilde{p}_\theta(y \mid x_j)} \frac{p_\theta(x_{j-1} \mid x_j)}{\tilde{p}_\theta(x_{j-1} \mid x_j, y)} \tilde{p}_\theta(x_{j-1} \mid x_j, y), \quad (22)$$

$$= \tilde{p}_\theta(y \mid x_K) p_K(x_K) \prod_{j=s}^k p_\theta(x_{j-1} \mid x_k), \quad (23)$$

$$= \tilde{p}_\theta(y \mid x_{s-1}) p_\theta(x_{s-1:K}), \quad (24)$$

$$= p(x_{s-1:K}, y). \quad (25)$$

And therefore:

$$\nu(x_{s:K}) = p(x_{s-1:K} \mid y), \quad (26)$$

$$\nu(x_{0:K}) = p(x_{0:K} \mid y). \quad (27)$$

### A.3. Pseudo-Bootstrap Formulation

For the pBS formulation of the FK process, we use the following:

$$\begin{aligned} M_K(x_K) &= p_K(x_K), & M_{j-1}(x_{j-1} \mid x_j) &= \tilde{p}_\theta(x_{j-1} \mid x_j, y), \\ G_K(x_K) &= \tilde{p}_\theta(y \mid x_K), & G_{j-1}(x_j, x_{j-1}) &= \frac{\tilde{p}_\theta(y \mid x_{j-1})}{\tilde{p}_\theta(y \mid x_j)}. \end{aligned}$$

Substituting these into equation 21:

$$\nu(x_{s:K}) \propto \tilde{p}_\theta(y \mid x_K) p_K(x_K) \prod_{j=s}^k \frac{\tilde{p}_\theta(y \mid x_{j-1})}{\tilde{p}_\theta(y \mid x_j)} \tilde{p}_\theta(x_{j-1} \mid x_j, y), \quad (28)$$

$$= \tilde{p}_\theta(x_{s-1:K}, y) \tilde{p}_\theta(y \mid x_{s-1}). \quad (29)$$

### A.4. Pseudocode

#### A.4.1. GEM PROPOSAL PSEUDOCODE

##### Algorithm 2 GEM Algorithm

**Require:**  $D_\theta(x; \sigma)$ ,  $\sigma_k, \sigma_{k-1}, x_k, \alpha$

- 1: Sample  $\epsilon_k \sim \mathcal{N}(0, I)$
- 2:  $d_k \leftarrow \frac{x_k - D_\theta(x_k, \sigma_k)}{\sigma_k}$
- 3:  $x_{k-1} \leftarrow x_k + (\sigma_{k-1}^2 - \sigma_k^2)d_k + \sqrt{\sigma_{k-1}^2 - \sigma_k^2}\epsilon_k$
- 4:  $x_{k-1} \leftarrow x_{k-1} - (\sigma_{k-1}^2 - \sigma_k^2)\nabla_{x_k} \log \tilde{p}_\theta(y \mid x_k)$
- 5: **return**  $x_{k-1}$

#### A.4.2. SOSAG PROPOSAL PSEUDOCODE

##### Algorithm 3 SOSaG Proposal

**Require:**  $D_\theta(x; \sigma)$ ,  $\sigma_k, \sigma_{k-1}, x_k, \gamma_k$

- 1: Sample  $\epsilon_k \sim \mathcal{N}(0, I)$
- 2:  $\hat{\sigma}_k \leftarrow \sigma_k + \gamma_k \sigma_k$
- 3:  $\hat{x}_k \leftarrow x_k + \sqrt{\hat{\sigma}_k^2 - \sigma_k^2}\epsilon_k$
- 4:  $d_k \leftarrow \frac{\hat{x}_k - D_\theta(\hat{x}_k, \hat{\sigma}_k)}{\hat{\sigma}_k}$
- 5:  $x_{k-1} \leftarrow \hat{x}_k + (\sigma_{k-1} - \hat{\sigma}_k) d_k$
- 6: **if**  $\sigma_k \neq 0$  **then**
- 7:      $d_{k-1} \leftarrow \frac{x_{k-1} - D_\theta(x_{k-1}, \sigma_{k-1})}{\sigma_{k-1}}$
- 8:      $x_{k-1} \leftarrow \hat{x}_k + (\sigma_{k-1} - \hat{\sigma}_k) \left( \frac{1}{2}d_k + \frac{1}{2}d_{k-1} \right)$
- 9: **end if**
- 10:  $x_{k-1} \leftarrow x_{k-1} - (\sigma_{k-1}^2 - \sigma_k^2)\nabla_{\hat{x}_k} \log \tilde{p}_\theta(y \mid \hat{x}_k)$
- 11: **return**  $x_{k-1}$

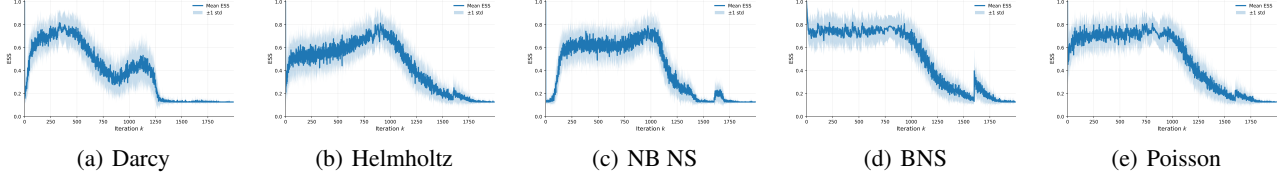


Figure 3. Averaged ESS for the EM TDS algorithm ( $\beta = 0$ ) across 20 runs. We can see that the sampler degenerates towards the end of the sampling process often leading to only one particle contributing to the target estimate.

## A.5. SMC and EA

As we can see in Figure 3, The TDS with an GEM proposal degenerates towards the end of the sampling run, often leading to only one particle contributing to the estimate of the target.

Illustrated in Fig. 4, a larger variance (smaller  $\beta$ ) allows multiple particles to attain comparable likelihoods, resulting in a higher ESS. Reducing the variance causes the likelihood to concentrate on a single particle, leading to ESS collapse. In the limit  $\beta \rightarrow 0$ , the ESS converges to one particle and the SMC sampler behaves similarly to an evolutionary algorithm (EA), such as the  $1 + \lambda$  EA (Yu & Gen, 2010; Bäck & Schwefel, 1993). In this regime, a single particle generates multiple proposals, which are evaluated and selectively propagated.

## B. Supplementary Experimental Design Material

### B.1. PDE Equation Details

#### B.1.1. BENCHMARK PDE DETAILS

**Darcy Flow:** In Darcy flow, we solve for the pressure field  $u(c)$  given the permeability field  $a(c)$  of a specific medium  $-\nabla \cdot (a(c)\nabla u(c)) = s(c)$

$$\begin{aligned} -\nabla \cdot (a(c)\nabla u(c)) &= s(c), \quad c \in \Omega \\ u(c) &= 0, \quad c \in \partial\Omega, \end{aligned} \tag{30}$$

and  $s(c)$  is a source term such as a forcing function. For these experiments, we set  $s(c) = 1$ .

**Inhomogeneous Helmholtz/Poisson Equation:** In the inhomogeneous Helmholtz equation we solve for the wave field  $u(c)$  given a forcing term  $a(c)$  which describes wave propagation:

$$\begin{aligned} \nabla^2 u(c) + k^2 u(c) &= a(c), \quad c \in \Omega \\ u(c) &= 0, \quad c \in \partial\Omega. \end{aligned} \tag{31}$$

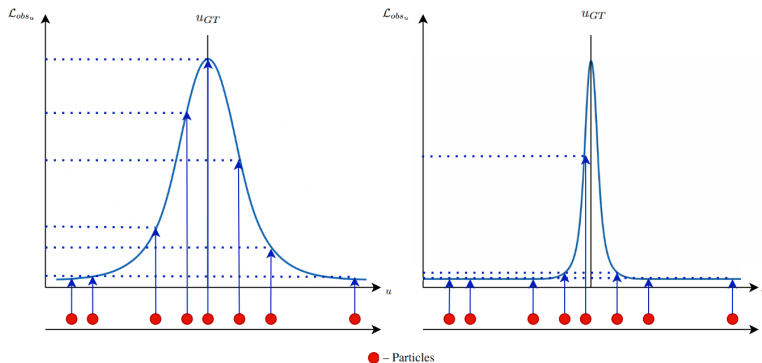


Figure 4. Example likelihood values for the same particles generated by SMC. The figure on the left shows the likelihood values with a larger variance, while the left figure shows the likelihood values with a smaller variance.

$k$  is a constant (wavenumber) and  $a(c)$  is a piecewise constant function. Note that when  $k = 0$ , this reduces to the Poisson equation:

$$\begin{aligned} \nabla^2 u(c) &= a(c), & c \in \Omega \\ u(c) &= 0, & c \in \partial\Omega. \end{aligned} \quad (32)$$

**Non-Bounded Incompressible Navier–Stokes:** The following describes the vorticity formulation of the non-bounded Navier–Stokes equation:

$$\begin{aligned} \frac{\partial w(c, \tau)}{\partial \tau} + v(c, \tau) \cdot \nabla w(c, \tau) &= \nu \nabla w(c, \tau) + q(c), & c \in \Omega, & \tau \in [0, \mathcal{T}], \\ \nabla \cdot v(c, \tau) &= 0, & c \in \Omega, & \tau \in [0, \mathcal{T}], \end{aligned} \quad (33)$$

where  $w = \nabla \times v$  is the vorticity.  $v(c, \tau)$  is the velocity at  $c$  at time  $\tau$ .  $q(c)$  again is a forcing term but represented as a field. We follow the same set up as (Huang et al., 2024), setting  $\nu = 1 \times 10^{-3}$  and learning the joint distribution of  $w_0$  and  $w_{\mathcal{T}}$ . The dynamics are simulated over  $\mathcal{T} = 10$  time steps which is equivalent to one second. The guidance is simplified to  $f = \nabla \cdot w(c, \tau)$  as we cannot compute the PDE loss from 33 with our model outputs.

**Bounded Incompressible Navier–Stokes:** We consider the bounded 2D Navier–Stokes equation:

$$\begin{aligned} \frac{\partial v(c, \tau)}{\partial \tau} + v(c, \tau) \cdot \nabla v(c, \tau) + \frac{1}{\rho} \nabla p &= \nu \nabla^2 v(c, \tau), & c \in \Omega, & \tau \in [0, \mathcal{T}], \\ \nabla \cdot v(c, \tau) &= 0, & c \in \Omega, & \tau \in [0, \mathcal{T}], \end{aligned} \quad (34)$$

where  $\rho = 1$  and  $\nu = 1 \times 10^{-3}$ . Again following the data generation process from (Huang et al., 2024), 2D cylinders of random radius and points are generated inside the grid. We learn the joint distribution of  $v_0, v_{\mathcal{T}}$  where  $\mathcal{T} = 4$  and this simulates 0.4 seconds. Similarly to the Nonbounded case, we use  $f = \nabla \cdot v(c, \tau)$ .

### B.1.2. REACTION–DIFFUSION EQUATIONS (2-SPECIES AND 3-SPECIES)

We now explain the 2SRD and 3SRD PDE equations with periodic boundary conditions.

**Two-species reaction–diffusion equation (Gray–Scott):** We consider a two-species reaction–diffusion (RD) system with solution fields  $u(c, \tau)$  and  $v(c, \tau)$  describing the concentrations of two interacting species. The dynamics are given by the Gray–Scott model:

$$\begin{aligned} \frac{\partial u(c, \tau)}{\partial \tau} &= D_u \Delta u(c, \tau) - u(c, \tau)v(c, \tau)^2 + F(1 - u(c, \tau)), & c \in \Omega, & \tau \in [0, \mathcal{T}], \\ \frac{\partial v(c, \tau)}{\partial \tau} &= D_v \Delta v(c, \tau) + u(c, \tau)v(c, \tau)^2 - (F + r)v(c, \tau), & c \in \Omega, & \tau \in [0, \mathcal{T}]. \end{aligned} \quad (35)$$

Here  $D_u$  and  $D_v$  are diffusivities,  $F$  is a feed rate and  $r$  is a removal rate. The nonlinear coupling term  $uv^2$  models autocatalytic production of  $v$  at the expense of  $u$ . In our experiments we set  $F = 0.035$  and  $r = 0.060$ . We simulate the system over  $\mathcal{T} = 1$  second, recording 10 evenly spaced time steps, and generate trajectories using FEM with time step  $1 \times 10^{-4}$ . Initial conditions are sampled as a perturbed uniform state with a centered square perturbation:  $u_0(c) \approx 1$  and  $v_0(c) \approx 0$  throughout the domain, except on a centered patch where  $u_0(c) \approx 0.5$  and  $v_0(c) \approx 0.25$ , with small additive Gaussian noise. We learn the joint distribution of the initial and final states  $(u_0, v_0)$  and  $(u_{\mathcal{T}}, v_{\mathcal{T}})$ .

We define the PDE guidance function as the reaction–diffusion residual  $f = (f_u, f_v)$ , where  $f_u = \partial_{\tau} u - D_u \Delta u + uv^2 - F(1 - u)$  and  $f_v = \partial_{\tau} v - D_v \Delta v - uv^2 + (F + r)v$ .

**Three-species reaction–diffusion equation:** We also consider a three-species reaction–diffusion system with solution fields  $u(c, \tau)$ ,  $v(c, \tau)$ , and  $z(c, \tau)$  governed by diffusion and competitive interactions:

$$\begin{aligned} \frac{\partial u(c, \tau)}{\partial \tau} &= \nabla \cdot (D_u \nabla u(c, \tau)) + u(c, \tau) \left(1 - u(c, \tau) - a_{12}v(c, \tau) - a_{13}z(c, \tau)\right), & c \in \Omega, & \tau \in [0, \mathcal{T}], \\ \frac{\partial v(c, \tau)}{\partial \tau} &= \nabla \cdot (D_v \nabla v(c, \tau)) + v(c, \tau) \left(1 - v(c, \tau) - a_{21}u(c, \tau) - a_{23}z(c, \tau)\right), & c \in \Omega, & \tau \in [0, \mathcal{T}], \\ \frac{\partial z(c, \tau)}{\partial \tau} &= \nabla \cdot (D_z \nabla z(c, \tau)) + z(c, \tau) \left(1 - z(c, \tau) - a_{31}u(c, \tau) - a_{32}v(c, \tau)\right), & c \in \Omega, & \tau \in [0, \mathcal{T}], \end{aligned} \quad (36)$$

Here  $D_u$ ,  $D_v$ , and  $D_z$  denote diffusion coefficients. Here  $a_{ij} \geq 0$  are competition coefficients quantifying how strongly species  $j$  inhibits species  $i$ , and we collect them in a coupling matrix  $A = (a_{ij}) \in \mathbb{R}^{3 \times 3}$  (with  $a_{11} = a_{22} = a_{33} = 0$ ). In our data generation procedure, we sample the dominant cyclic interaction terms  $a_{12}, a_{23}, a_{31} \sim \mathcal{U}(1.2, 2.0)$  and the remaining cross-interaction terms  $a_{13}, a_{21}, a_{32} \sim \mathcal{U}(0.3, 0.8)$ .  $u_0(c) \approx 0.6$ ,  $v_0(c) \approx 0.2$ , and  $z_0(c) \approx 0.2$  throughout the domain, except on three localized patches near the domain center where  $u_0(c) \approx 0.9$ ,  $v_0(c) \approx 0.7$ , and  $z_0(c) \approx 0.7$ , respectively, with small additive Gaussian noise. We learn the joint distribution of the initial and final states  $(u_0, v_0, z_0)$  and  $(u_{\mathcal{T}}, v_{\mathcal{T}}, z_{\mathcal{T}})$ .

Similarly, we define the PDE guidance function as the reaction-diffusion residual  $f = (f_u, f_v, f_z)$ , where  $f_u = \partial_{\tau}u - D_u\Delta u - u(1-u-a_{12}v-a_{13}z)$ ,  $f_v = \partial_{\tau}v - D_v\Delta v - v(1-v-a_{21}u-a_{23}z)$ , and  $f_z = \partial_{\tau}z - D_z\Delta z - z(1-z-a_{31}u-a_{32}v)$ .

## B.2. Model Training and Evaluation

For the benchmark PDEs we used the pretrained model parameters from [Huang et al. \(2024\)](#). The model is the modified UNet ([Ronneberger et al., 2015](#)) implementation used in [Song et al. \(2021\)](#) with each model trained on 50000 training images for each experiment. We refer the user to [Huang et al. \(2024\)](#) for further details on this.

For the multiphysics equations, we generated our own data using FEM to train the model architecture. For both the 2 species and 3 species variants, we generated 10000 training images and trained the model by doing 100,000 gradient passes over the dataset. A single A100 NVIDIA GPU was used for training.

For the evaluation, we generated 1000 test images and randomly chose a trajectory and then evaluated on the midpoint. We repeated this 20 times for each experiment and method, keeping the same image and known observations but with a different starting seed for particle initialization.

It is worth noting that we do not believe that our model was optimized with a scheme that leads to the optimal parameters. When training was terminated, the loss was still decreasing, albeit slowly. Therefore we think we all models could have superior results by optimizing this process. However, we felt that this task was outside the purview of this work as all methods including baselines still obtained good results. We also believe that there are potentially better architectures in the literature that would work better as a model prior than what we have chosen. The [Song et al. \(2021\)](#) was used for convenience and as that is what our baselines comparisons used for the pretrained models.

We found during some of our training runs that increasing  $K$  improved all results across every sampling method, which is expected but the result was more pronounced for the stochastic sampling methods. We decided to use  $K = 2000$  for each experiment and method, however we feel that experimenting with this parameter would be fruitful for more optimized results in future work. This obviously comes at an increased wall-clock time cost.

## C. Further Results

Table 3 gives the full results for the benchmark PDE experiments where the likelihood associated with  $\beta$  is included. Table 4 shows the results for the same set of experiments but with  $\beta = 0$ . We see that for the stochastic methods, using  $\beta > 0$  when calculating the importance weights leads to a significant drop in the relative error of the solution field  $u$ .

Table 5 gives an ablation study for increasing sample sizes. We see that generally, as expected, more samples tend to lead to a lower relative error. This motivates the need for a multi-GPU implementation of the sampling process if this method is applied to a real world scenario, in order to produce the best results.

Table 3. Performance and accuracy across PDE benchmarks. **Likelihood Included** ( $\beta > 0$ )

Experiment	Method	Time (s)	Rel. Error (a)	Rel. Error (u)
Darcy	DiffPDE	276.23 $\pm$ 0.8968	0.0347 $\pm$ 0.0022	0.0331 $\pm$ 0.0091
	DiffPDE-NoG	275.35 $\pm$ 0.5490	0.4948 $\pm$ 0.1371	0.3322 $\pm$ 0.0891
	EM (Proposal)	<b>239.88 <math>\pm</math> 0.5116</b>	0.0340 $\pm$ 0.0034	0.0308 $\pm$ 0.0145
	EM (pBS)	1173.99 $\pm$ 0.5676	0.0185 $\pm$ 0.0023	<b>0.0103 <math>\pm</math> 0.0077</b>
	EM (Guided)	1170.60 $\pm$ 0.6032	0.0186 $\pm$ 0.0024	0.0122 $\pm$ 0.0122
	SOSaG (Proposal)	285.46 $\pm$ 1.2361	0.0335 $\pm$ 0.0029	0.0294 $\pm$ 0.0082
	SOSaG (pBS)	1284.33 $\pm$ 1.2706	<b>0.0181 <math>\pm</math> 0.0017</b>	0.0115 $\pm$ 0.0082
Helmholtz	DiffPDE	274.38 $\pm$ 0.96	0.1333 $\pm$ 0.0047	0.1661 $\pm$ 0.1023
	DiffPDE-NoG	276.65 $\pm$ 0.43	1.5996 $\pm$ 0.3675	1.8485 $\pm$ 0.6266
	EM (Proposal)	<b>234.90 <math>\pm</math> 0.42</b>	0.1368 $\pm$ 0.0039	0.1275 $\pm$ 0.0808
	EM (pBS)	1163.51 $\pm$ 2.10	0.1279 $\pm$ 0.0039	<b>0.0296 <math>\pm</math> 0.0017</b>
	EM (Guided)	1165.23 $\pm$ 1.22	0.1269 $\pm$ 0.0042	0.0298 $\pm$ 0.0015
	SOSaG (Proposal)	287.10 $\pm$ 0.83	0.1356 $\pm$ 0.0044	0.1390 $\pm$ 0.0750
	SOSaG (pBS)	1261.96 $\pm$ 1.28	<b>0.1249 <math>\pm</math> 0.0037</b>	0.0299 $\pm$ 0.0018
Bounded NS	DiffPDE	289.63 $\pm$ 0.86	0.0237 $\pm$ 0.0084	0.0283 $\pm$ 0.0072
	DiffPDE-NoG	288.71 $\pm$ 0.54	0.5104 $\pm$ 0.1944	0.5032 $\pm$ 0.1764
	EM (Proposal)	<b>239.41 <math>\pm</math> 1.08</b>	0.0257 $\pm$ 0.0096	0.0270 $\pm$ 0.0093
	EM (pBS)	1089.12 $\pm$ 1.02	0.0797 $\pm$ 0.0025	<b>0.0175 <math>\pm</math> 0.0009</b>
	EM (Guided)	1171.56 $\pm$ 1.25	0.0228 $\pm$ 0.0060	0.0236 $\pm$ 0.0055
	SOSaG (Proposal)	285.81 $\pm$ 1.27	0.0212 $\pm$ 0.0067	0.0238 $\pm$ 0.0064
	SOSaG (pBS)	1284.12 $\pm$ 2.46	<b>0.0207 <math>\pm</math> 0.0046</b>	0.0229 $\pm$ 0.0037
Non-Bounded NS	DiffPDE	289.63 $\pm$ 0.59	0.1021 $\pm$ 0.0047	0.0522 $\pm$ 0.0057
	DiffPDE-NoG	288.55 $\pm$ 0.81	1.5818 $\pm$ 0.2157	1.7163 $\pm$ 0.2630
	EM (Proposal)	<b>237.99 <math>\pm</math> 0.63</b>	0.1029 $\pm$ 0.0053	0.0547 $\pm$ 0.0065
	EM (pBS)	1089.12 $\pm$ 1.02	0.0797 $\pm$ 0.0025	0.0175 $\pm$ 0.0009
	EM (Guided)	1166.78 $\pm$ 0.88	0.0794 $\pm$ 0.0020	<b>0.0174 <math>\pm</math> 0.0006</b>
	SOSaG (Proposal)	284.93 $\pm$ 0.68	0.1034 $\pm$ 0.0058	0.0552 $\pm$ 0.0066
	SOSaG (pBS)	1266.11 $\pm$ 1.20	<b>0.0781 <math>\pm</math> 0.0024</b>	<b>0.0174 <math>\pm</math> 0.0007</b>
Poisson	DiffPDE	286.10 $\pm$ 0.77	0.1125 $\pm$ 0.0032	0.0672 $\pm$ 0.0336
	DiffPDE-NoG	286.08 $\pm$ 1.19	1.5687 $\pm$ 0.3551	1.6097 $\pm$ 0.5281
	EM (Proposal)	<b>236.43 <math>\pm</math> 0.91</b>	0.1127 $\pm$ 0.0032	0.0717 $\pm$ 0.0422
	EM (pBS)	1186.86 $\pm$ 5.64	0.1050 $\pm$ 0.0023	<b>0.0213 <math>\pm</math> 0.0011</b>
	EM (Guided)	1162.80 $\pm$ 1.05	0.1051 $\pm$ 0.0028	0.0214 $\pm$ 0.0011
	SOSaG (Proposal)	280.92 $\pm$ 0.73	0.1134 $\pm$ 0.0038	0.0912 $\pm$ 0.0521
	SOSaG (pBS)	1265.76 $\pm$ 2.16	<b>0.1040 <math>\pm</math> 0.0025</b>	0.0215 $\pm$ 0.0010

Table 4. Performance and accuracy across PDE benchmarks. **Likelihood Not Included** ( $\beta = 0$ ).

Experiment	Method	Time (s)	Rel. Error (a)	Rel. Error (u)
Darcy	DiffPDE	276.66 $\pm$ 1.20	0.0350 $\pm$ 0.0021	0.0367 $\pm$ 0.0100
	DiffPDE-NoG	275.94 $\pm$ 0.25	0.4908 $\pm$ 0.1229	0.3322 $\pm$ 0.0833
	EM (Proposal)	<b>240.10 <math>\pm</math> 0.44</b>	0.0344 $\pm$ 0.0039	0.0345 $\pm$ 0.0204
	EM (pBS)	1162.68 $\pm$ 0.80	<b>0.0328 <math>\pm</math> 0.0024</b>	<b>0.0279 <math>\pm</math> 0.0067</b>
	EM (Guided)	1174.02 $\pm$ 0.54	0.0337 $\pm$ 0.0035	0.0372 $\pm$ 0.0173
	SOSaG (Proposal)	286.54 $\pm$ 1.32	0.0339 $\pm$ 0.0025	0.0289 $\pm$ 0.0069
	SOSaG (pBS)	1371.17 $\pm$ 0.57	0.0331 $\pm$ 0.0036	<b>0.0279 <math>\pm</math> 0.0074</b>
Helmholtz	DiffPDE	275.09 $\pm$ 1.20	0.1330 $\pm$ 0.0043	0.2168 $\pm$ 0.1175
	DiffPDE-NoG	276.65 $\pm$ 0.45	1.6770 $\pm$ 0.3269	2.0643 $\pm$ 0.5188
	EM (Proposal)	<b>235.22 <math>\pm</math> 0.42</b>	0.1359 $\pm$ 0.0039	<b>0.1203 <math>\pm</math> 0.0876</b>
	EM (pBS)	1167.80 $\pm$ 0.79	0.1380 $\pm$ 0.0041	0.1807 $\pm$ 0.0899
	EM (Guided)	1168.11 $\pm$ 0.67	<b>0.1326 <math>\pm</math> 0.0034</b>	0.2529 $\pm$ 0.1273
	SOSaG (Proposal)	287.33 $\pm$ 0.95	0.1349 $\pm$ 0.0050	0.1288 $\pm$ 0.0830
	SOSaG (pBS)	1362.96 $\pm$ 0.87	0.1342 $\pm$ 0.0055	0.1522 $\pm$ 0.0674
Bounded NS	DiffPDE	289.64 $\pm$ 1.24	0.0245 $\pm$ 0.0084	0.0280 $\pm$ 0.0078
	DiffPDE-NoG	289.02 $\pm$ 0.73	0.5641 $\pm$ 0.2043	0.5542 $\pm$ 0.1879
	EM (Proposal)	<b>239.51 <math>\pm</math> 1.39</b>	0.0233 $\pm$ 0.0089	0.0273 $\pm$ 0.0085
	EM (pBS)	1161.16 $\pm$ 0.77	0.0206 $\pm$ 0.0044	0.0232 $\pm$ 0.0030
	EM (Guided)	1166.01 $\pm$ 0.56	0.0203 $\pm$ 0.0045	0.0237 $\pm$ 0.0036
	SOSaG (Proposal)	286.96 $\pm$ 1.09	0.0229 $\pm$ 0.0068	0.0257 $\pm$ 0.0077
	SOSaG (pBS)	1364.42 $\pm$ 1.37	<b>0.0197 <math>\pm</math> 0.0045</b>	<b>0.0220 <math>\pm</math> 0.0037</b>
Non-Bounded NS	DiffPDE	289.81 $\pm$ 0.68	<b>0.1024 <math>\pm</math> 0.0052</b>	<b>0.0510 <math>\pm</math> 0.0058</b>
	DiffPDE-NoG	288.93 $\pm$ 1.15	1.6105 $\pm$ 0.1831	1.7493 $\pm$ 0.2254
	EM (Proposal)	<b>237.78 <math>\pm</math> 0.92</b>	0.1035 $\pm$ 0.0058	0.0553 $\pm$ 0.0070
	EM (pBS)	1171.67 $\pm$ 0.79	0.1032 $\pm$ 0.0053	0.0560 $\pm$ 0.0056
	EM (Guided)	1171.27 $\pm$ 2.06	0.1026 $\pm$ 0.0050	0.0575 $\pm$ 0.0043
	SOSaG (Proposal)	285.41 $\pm$ 0.39	0.1045 $\pm$ 0.0051	0.0570 $\pm$ 0.0068
	SOSaG (pBS)	1366.57 $\pm$ 1.24	0.1026 $\pm$ 0.0045	0.0547 $\pm$ 0.0055
Poisson	DiffPDE	286.58 $\pm$ 1.00	0.1126 $\pm$ 0.0031	0.0731 $\pm$ 0.0308
	DiffPDE-NoG	287.03 $\pm$ 1.35	1.5752 $\pm$ 0.3550	1.6518 $\pm$ 0.4897
	EM (Proposal)	<b>236.49 <math>\pm</math> 1.15</b>	<b>0.1121 <math>\pm</math> 0.0032</b>	<b>0.0632 <math>\pm</math> 0.0345</b>
	EM (pBS)	1164.99 $\pm$ 0.56	0.1122 $\pm$ 0.0031	0.0727 $\pm$ 0.0375
	EM (Guided)	1170.93 $\pm$ 1.17	0.1128 $\pm$ 0.0032	0.1114 $\pm$ 0.0617
	SOSaG (Proposal)	280.77 $\pm$ 1.01	0.1124 $\pm$ 0.0032	0.0756 $\pm$ 0.0368
	SOSaG (pBS)	1261.40 $\pm$ 2.15	0.1139 $\pm$ 0.0035	0.0640 $\pm$ 0.0239

Table 5. Sample size ablation study for Darcy Flow.

Experiment	Method (Batch Size)	Time (s)	Rel. Error (a)	Rel. Error (u)
Darcy $\beta > 0$	EM (1)	<b>239.88 <math>\pm</math> 0.51</b>	0.0340 $\pm$ 0.0034	0.0308 $\pm$ 0.0145
	EM (2)	353.38 $\pm$ 0.30	0.0339 $\pm$ 0.0029	0.0314 $\pm$ 0.0108
	EM (4)	656.23 $\pm$ 0.46	0.0203 $\pm$ 0.0016	0.0116 $\pm$ 0.0096
	EM (8)	1170.60 $\pm$ 0.60	0.0186 $\pm$ 0.0024	0.0122 $\pm$ 0.0122
	SOSaG (1)	285.46 $\pm$ 1.24	0.0335 $\pm$ 0.0029	0.0294 $\pm$ 0.0082
	SOSaG (2)	417.90 $\pm$ 0.95	0.0333 $\pm$ 0.0033	0.0292 $\pm$ 0.0087
	SOSaG (4)	757.22 $\pm$ 0.97	0.0194 $\pm$ 0.0018	<b>0.0101 <math>\pm</math> 0.0018</b>
	SOSaG (8)	1284.33 $\pm$ 1.27	<b>0.0181 <math>\pm</math> 0.0017</b>	0.0115 $\pm$ 0.0082
	EM (1)	<b>240.10 <math>\pm</math> 0.44</b>	0.0344 $\pm$ 0.0039	0.0345 $\pm$ 0.0204
	EM (2)	353.25 $\pm$ 1.27	0.0340 $\pm$ 0.0028	0.0291 $\pm$ 0.0052
Darcy $\beta = 0$	EM (4)	607.10 $\pm$ 0.84	0.0351 $\pm$ 0.0039	0.0393 $\pm$ 0.0216
	EM (8)	1174.02 $\pm$ 0.54	0.0337 $\pm$ 0.0035	0.0372 $\pm$ 0.0173
	SOSaG (1)	286.54 $\pm$ 1.32	0.0339 $\pm$ 0.0025	0.0289 $\pm$ 0.0069
	SOSaG (2)	413.57 $\pm$ 1.46	0.0335 $\pm$ 0.0021	0.0294 $\pm$ 0.0071
	SOSaG (4)	710.52 $\pm$ 1.02	0.0333 $\pm$ 0.0031	0.0294 $\pm$ 0.0058
	SOSaG (8)	1371.17 $\pm$ 0.57	<b>0.0331 <math>\pm</math> 0.0036</b>	<b>0.0279 <math>\pm</math> 0.0074</b>

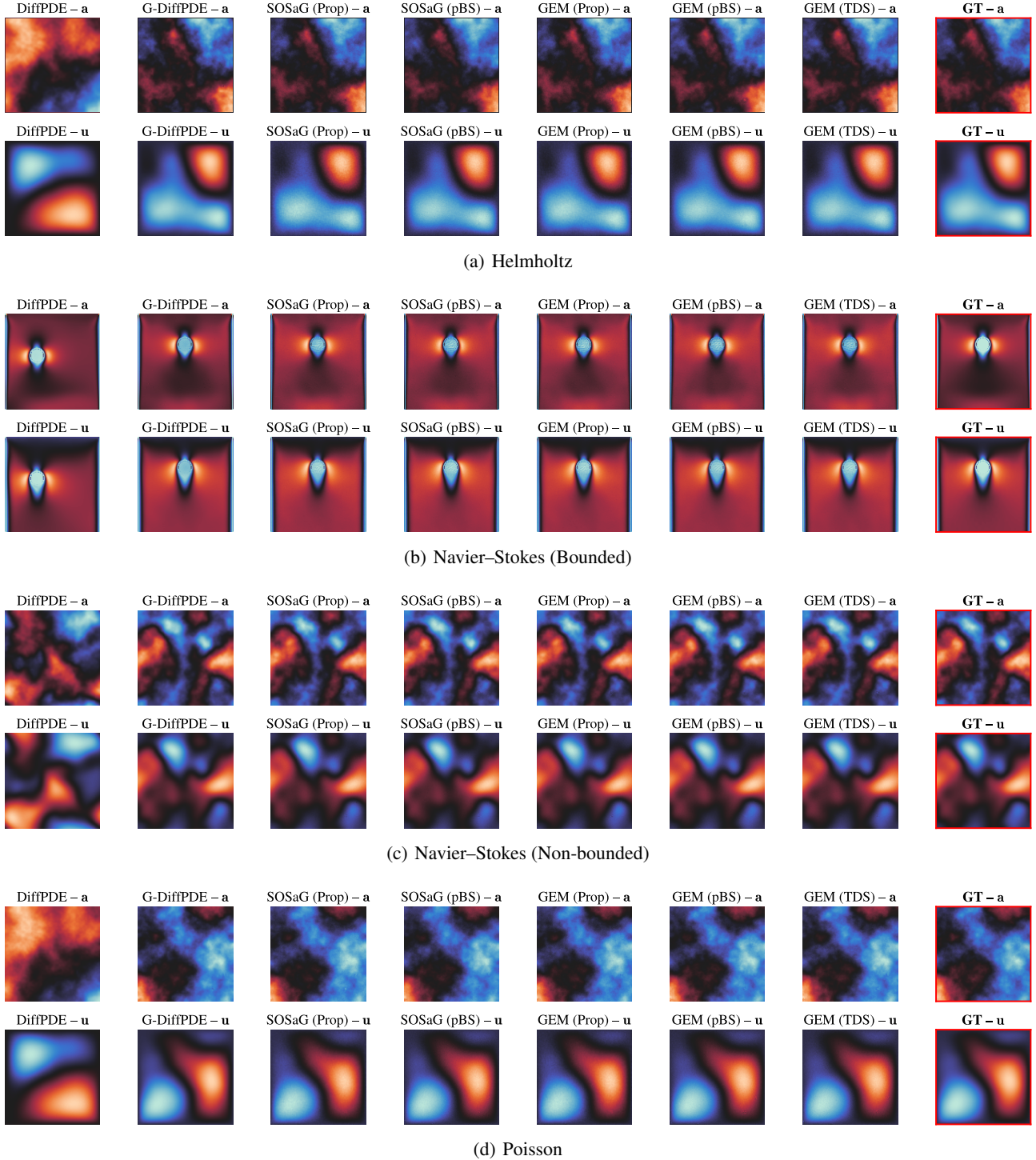


Figure 5. Reconstruction comparison for the benchmark PDE experiments. The top row shows the contour plots of the reconstruction of  $a$  while the bottom row shows the reconstruction of  $u$ . The final two plots on the right show the ground truth of the respective fields. The figures show a single example run of each method.

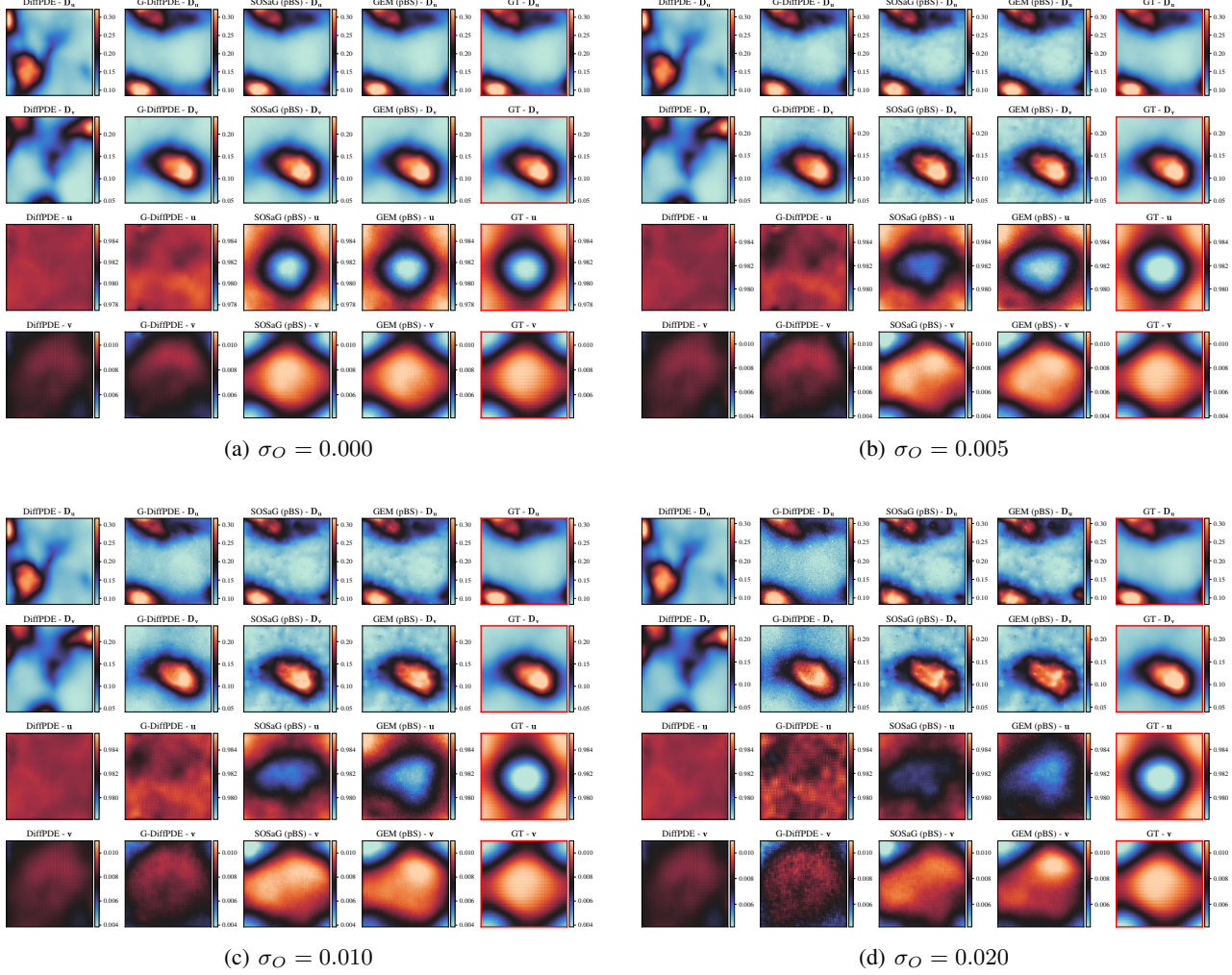


Figure 6. Reconstruction comparison for all 2SRD experiments across varying noise levels. The right most column show the ground truth contours. The figures show a single example run of each method.

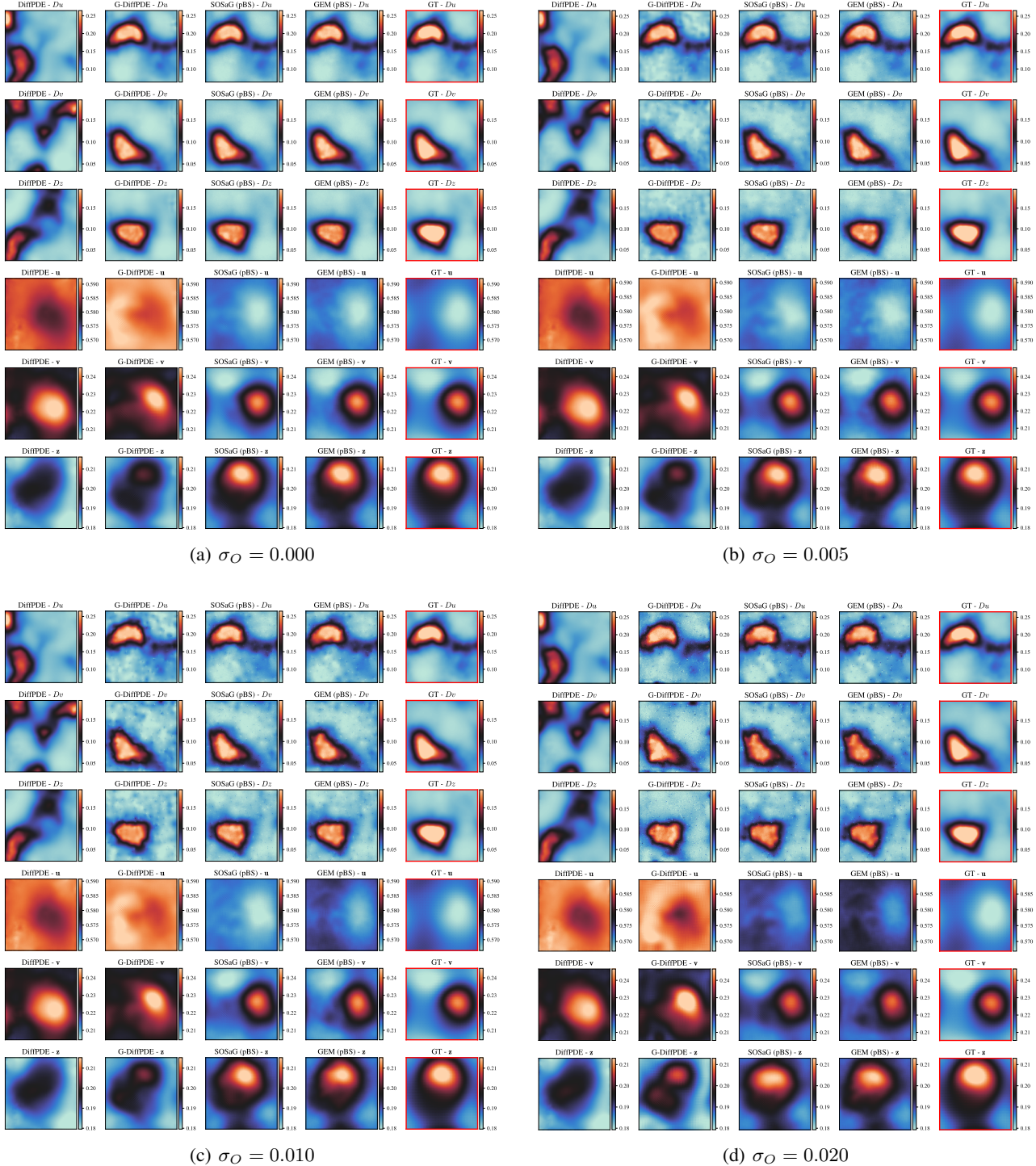


Figure 7. Reconstruction comparison for all 3SRD experiments across varying noise levels. The right most column show the ground truth contours. The figures show a single example run of each method.

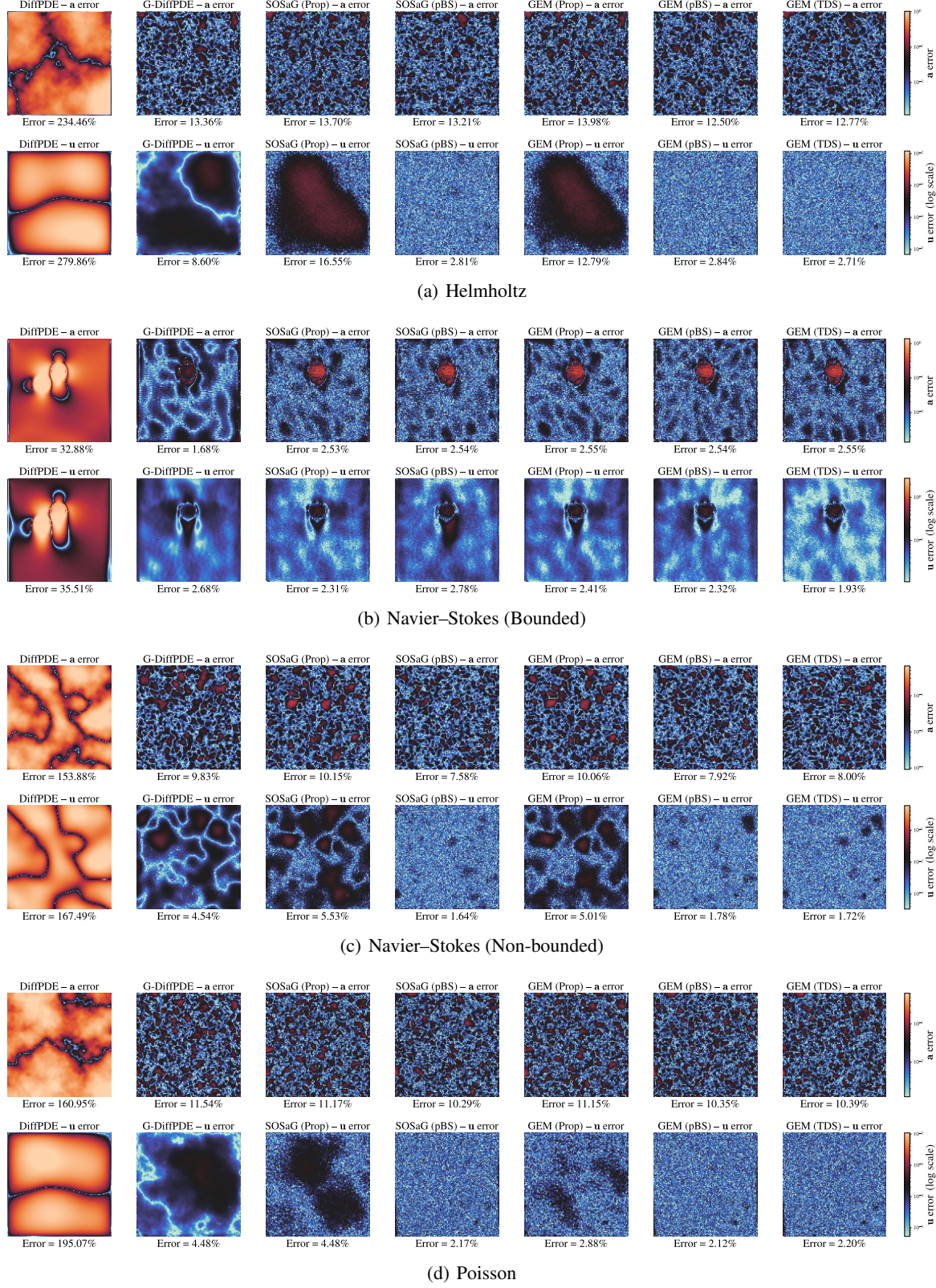


Figure 8. Corresponding error comparison panels for all PDE experiments: Helmholtz, Navier-Stokes bounded, Navier-Stokes non-bounded, and Poisson. The errors tend to be more erroneous near the high frequency information regions, this is most obvious in the Bounded Navier-Stokes case.

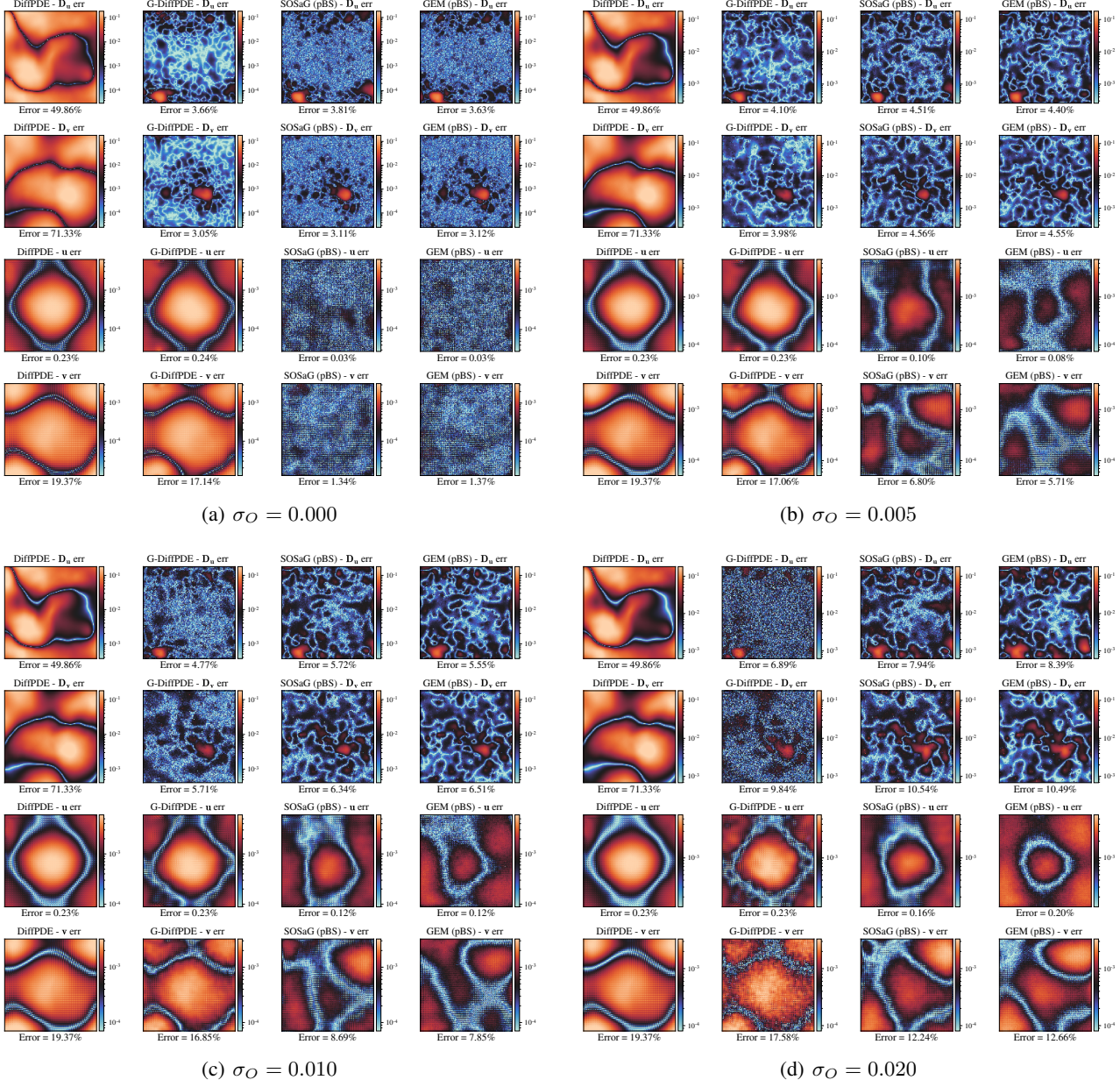


Figure 9. Corresponding error comparison panels for the 2SRD PDE system for the reconstructions. The highest error can be observed generally near the high frequency information regions, with this result being more pronounced with increasing levels of observation noise.

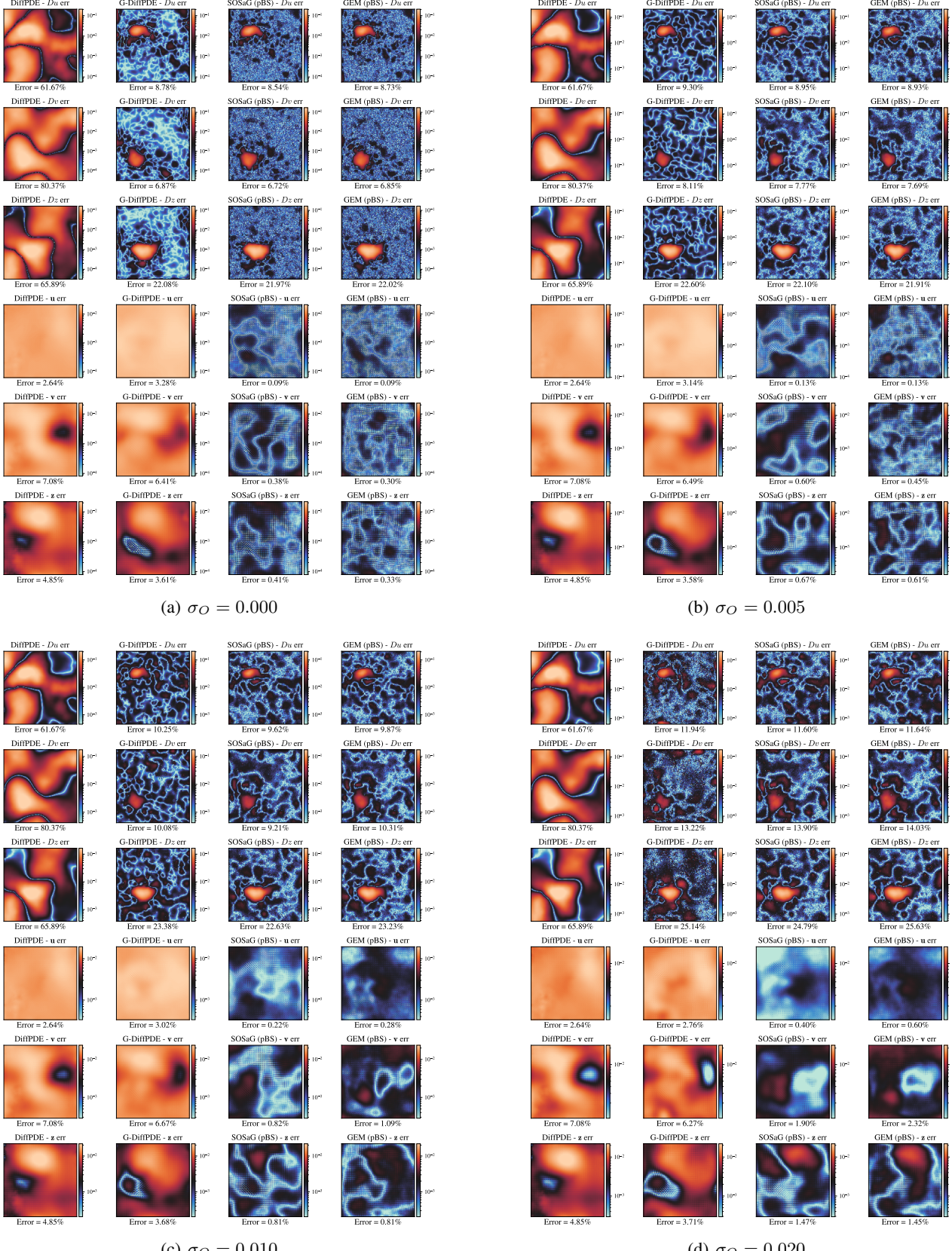


Figure 10. Error comparison panels for the 3SRD PDE system. Similarly to Figure 8 and Figure 9, we observe that generally the highest error regions are that near the high frequency information areas with the error increasing as we introduce more observation noise.